



Space borne tropospheric nitrogen dioxide (NO₂) observations from 2005-2020 over the Yangtze River Delta (YRD), China: variabilities, implications, and drivers

Hao Yin^{1,2}, Youwen Sun^{1,†}, Justus Notholt³, Mathias Palm³, and Cheng Liu^{2,4,5,6}

¹Key Laboratory of Environmental Optics and Technology, Anhui Institute of Optics and Fine Mechanics, HFIPS, Chinese Academy of Sciences, Hefei 230031, China

²Department of Precision Machinery and Precision Instrumentation, University of Science and Technology of China, Hefei 230026, China

³University of Bremen, Institute of Environmental Physics, P. O. Box 330440, 28334 Bremen, Germany

⁴Anhui Province Key Laboratory of Polar Environment and Global Change, University of Science and Technology of China, Hefei 230026, China

⁵Center for Excellence in Regional Atmospheric Environment, Institute of Urban Environment, Chinese Academy of Sciences, Xiamen 361021, China

⁶Key Laboratory of Precision Scientific Instrumentation of Anhui Higher Education Institutes, University of Science and Technology of China, Hefei 230026, China

[†]Correspondence to: Youwen Sun (ywsun@aiofm.ac.cn)

Abstract

Nitrogen dioxide (NO₂) is mainly affected by local emission and meteorology rather than long-range transport. Accurate knowledge of its long-term variabilities and drivers are significant for understanding the evolutions of economic and social development, anthropogenic emission, and the effectiveness of pollution control measures on regional scale. In this study, we quantify the long-term variabilities and the underlying drivers of NO₂ from 2005 to 2020 over the Yangtze River Delta (YRD), one of the most densely populated and highly industrialized city clusters in China, using OMI space borne observations and the multiple linear regression (MLR) model. We have compared the space borne tropospheric results to the surface in-situ data, yielding correlation coefficients of 0.8 to 0.9 over all megacities within the YRD. As a result, the tropospheric NO₂ column measurements can be used as representatives of near-surface conditions, and we thus only use ground-level meteorological data for MLR regression. The inter-annual variabilities of tropospheric NO₂ vertical column densities (VCDs) from 2005 to 2020 over the YRD can be divided into two stages. The first stage was from 2005 to 2011, which showed overall increasing trends with a wide range of (1.91 ± 1.50) to $(6.70 \pm 0.10) \times 10^{14}$ molecules/cm²·yr⁻¹ ($p < 0.01$) over the YRD. The second stage was from 2011 to 2020, which showed over all decreasing trends of (-6.31 ± 0.71) to $(-11.01 \pm 0.90) \times 10^{14}$ molecules/cm²·yr⁻¹ ($p < 0.01$) over each of the megacities. The seasonal cycles of tropospheric NO₂ VCDs over the YRD are mainly driven by meteorology (81.01% - 83.91%) except during winter when anthropogenic emission contributions are pronounced (16.09% - 18.99%). The inter annual variabilities of tropospheric NO₂ VCDs are mainly driven by anthropogenic emission (69.18% - 81.34%) except for a few years such as 2018 which are partly attributed to meteorology anomalies (39.07% - 91.51%). The increasing trends in tropospheric NO₂ VCDs from 2005 to 2011 over the YRD are mainly attributed to high energy consumption associated with rapid economic growth which cause significant increases in anthropogenic NO₂ emissions. The decreasing trends in



42 tropospheric NO₂ VCDs from 2011 to 2020 over the YRD are mainly attributed to the stringent
43 clean air measures which either adjust high energy industrial structure toward low energy industrial
44 structure or directly reduce pollutant emissions from different industrial sectors.

45 Keywords: OMI; nitrogen dioxide; Emissions; Meteorology; Multiple linear regression model

46 1. Introduction

47 As a major tropospheric pollutant, nitrogen dioxide (NO₂) not only threatens human health and
48 crop growth but also involves in a series of atmospheric photochemical reactions (Yin et al.,
49 2019; Wang et al., 2011; Geddes et al., 2012). NO₂ is a crucial precursor in the formation of ozone
50 (O₃), particulate matter (PM), acid rain, and photochemical smog in the troposphere (Yin et al.,
51 2021a; Lu et al., 2019a; Lu et al., 2019b; Sun et al., 2018). Since severe NO₂ pollution increases the
52 risk of respiratory disease and is highly associated with mortality (Meng et al., 2021; MacIntyre et
53 al., 2014; Tao et al., 2012), many countries take the NO₂ level as an important pollution indicator of
54 air quality (Xue et al., 2020). The sources of tropospheric NO₂ are mainly from anthropogenic
55 emissions through high temperature combustions, like transportation (vehicles, ships, and airplanes)
56 and industrial facilities (petrochemicals and power plants) (Zheng et al., 2018b; Chi et al., 2021; van
57 Geffen et al., 2015). Additional minor sources of NO₂ are attributed to natural emissions from
58 biogeochemical reaction in soil, volcanic eruption, and lightning (Bond et al., 2001; Zhang et al.,
59 2003; Lu et al., 2021). The dominant sink of tropospheric NO₂ is attributed to a chemical destruction
60 which first converts NO₂ into nitric acid (HNO₃) and peroxyacetyl nitrate (PAN) which then are by
61 dry or wet deposition (Browne et al., 2013). Due to a short lifetime of a few hours, tropospheric
62 NO₂ is heavily affected by local emissions and meteorology rather than long-range transport (Kim
63 et al., 2015; Cheng et al., 2012).

64 Many scientists have used a suite of active and passive observation technologies onboard
65 ground-based, vehicle-based, ship-based, airborne, or space borne platforms to assess the temporal-
66 spatial variabilities of NO₂ and identify their driving forces in different regions around the globe
67 (Richter et al., 2005; Jiang et al., 2018; Liu et al., 2018; Zhang et al., 2021; Schreier et al.,
68 2015; Shaiganfar et al., 2017). Among all observation technologies and platforms, space borne
69 remote sensing observations have their unique features. By validating with ground-based remote
70 sensing or balloon observations, space borne observations can provide global NO₂ dataset with a
71 reasonable accuracy. Typical space borne instruments include the SCIAMACHY, GOME, OMI, and
72 TROPOMI, which have been widely used in scientific investigations of global nitrogen cycle, O₃
73 formation regime, and regional pollution & transport, quantification of NO₂ emissions from biomass
74 burning regions, megacities, and industrial facilities, and validation of shipborne observations and
75 atmospheric chemical transport models (CTMs) (Richter et al., 2005; Bechle et al., 2013; Boersma
76 et al., 2011; Ghude et al., 2009; Lamsal et al., 2008). Using space borne observations to derive long
77 term trends of NO₂ and their drivers not only provides valuable information for evaluation of
78 regional emissions, but also improves our understanding of atmospheric evolutions. Richter et al.,
79 (2005) first investigated the inter annual variabilities of tropospheric NO₂ vertical column densities
80 (VCDs) from space with GOME and SCIAMACHY observations during 1996-2004. Richter et al.,
81 (2005) found substantial reductions in NO₂ VCDs over some areas of Europe and the USA, but a
82 highly significant increase of about 50%—with an accelerating trend in annual growth rate—over
83 the industrial areas of China. In a subsequent study, Ghude et al., (2009) found the same



phenomenon as those of Richter et al., (2005) with GOME and SCIAMACHY observations from 1996 to 2006, which disclosed that tropospheric NO₂ VCDs showed increasing trends over the rapid developing regions (China: $11 \pm 2.6\%/year$, South Asia: $1.76 \pm 1.1\%/year$, Middle East Africa: $2.3 \pm 1\%/year$) and decreasing or level-off trends over the developed regions (US: $-2 \pm 1.5\%/year$, Europe: $0.9 \pm 2.1\%/year$). With multiple satellite platforms including GOME, SCIAMACHY, OMI, and GOME-2, Hilboll et al., (2013) also found 5% to 10% yr⁻¹ of increasing trends for tropospheric NO₂ VCDs over eastern Asia during 1996 to 2011. With the OMI observations, Lamsal et al., (2015) have quantified the NO₂ trend from 2005 to 2013 over the US and Krotkov et al., (2016) have investigated the NO₂ trends over different countries for the period of 2005–2014.

Along with the great advances in social and economic development in recent decades, air quality in China has changed dramatically (Sun et al., 2020; Sun et al., 2021c; Yin et al., 2020; Yin et al., 2021c; Yin et al., 2021d). China has implemented a series of clean air measures in different stages to tackle air pollution across China. One of the landmark clean air measures could be the Action Plan on the Prevention and Control of Air Pollution implemented in 2013, which launched many stringent measures to improve air quality across China. These measures include the reduction of air pollutant emissions, the adjustment of industrial structure and energy mix, the establishment of early-warning systems and monitoring for air pollution, and other compulsive policies (China State Council, 2013). Both space borne and ground-based observations have witnessed the effectiveness of these successful policies. The OMI tropospheric NO₂ VCDs have been decreased by 21% from 2011 to 2015 over 48 cities of China (Liu et al., 2017). The national averaged surface NO₂ recorded by the China National Environmental Monitoring Center (CNEMC) network has significantly decreased from (16.68 ± 4.82) ppbv in 2013 to (11.29 ± 3.25) ppbv in 2020 (Lin et al., 2021).

In this study, we use tropospheric NO₂ VCDs from 2005–2020 provided by OMI to comprehensively evaluate the long-term trends, implications, and underlying drivers of NO₂ over the Yangtze River Delta (YRD, including Anhui, Jiangsu, Shanghai, and Zhejiang Provinces). In addition to anthropogenic emission, meteorology also drives NO₂ variability by affecting emissions, transport, chemical production, and scavenging. The relationships of NO₂ against meteorological variables are complex and are region and time dependent. In present work, we separate the contributions of meteorology and anthropogenic emission to the NO₂ variability by multiple linear regression (MLR) model over the major cities (Hefei, Nanjing, Suzhou, Shanghai, Hangzhou, Ningbo) within the YRD. As one of the three most densely populated and highly industrialized city clusters in China, the YRD has long been identified as a key region for air pollution mitigation. This study can not only improve our understanding of temporal spatial NO₂ evolutions in the atmosphere but also provides valuable information for future clean air policy. We introduce detailed descriptions of OMI and ground-level NO₂ products in section 2.1, and meteorological fields in section 2.2. The method for separating contributions of meteorology and anthropogenic emission is presented in section 2.3. Sections 3.1 and 3.2 analyze the temporal-spatial variabilities of tropospheric NO₂ from 2005 to 2020 over the YRD on provincial and megacity levels, respectively. A comparison between the OMI NO₂ product and the ground-level measurements is performed in section 3.3. We discuss the implications and underlying drivers of the variabilities of tropospheric NO₂ from 2005 to 2020 over the YRD in section 4. We conclude this study in section 5.

2. Data and method

2.1 Observation data



2.1.1 OMI NO₂ product

OMI is a hyperspectral atmospheric composition detection instrument onboard the National Aeronautics and Space Administration (NASA) Aura Earth Observing System (EOS) satellite launched in July, 2004 (Boersma et al., 2007). The EOS satellite flies over a low-Earth orbit at an altitude of about 710 km. The local overpass time (LT) of OMI satellite is about 13:30 in early afternoon. The retrieval micro window for NO₂ VCDs lies in between 405 nm and 465 nm with a spectral resolution of about 0.5 nm (Marchenko et al., 2015). The spatial resolution of OMI measurements is 13 × 24 km² at nadir. OMI provides observations of O₃, NO₂, SO₂, aerosol, cloud, HCHO, BrO, and OCIO with nearly daily global coverage (Levelt et al., 2006). The daily LV3 data product of tropospheric NO₂ VCDs data (GES DISC; <http://disc.sci.gsfc.nasa.gov>, last accessed: 1 September 2021) which is a gridded data with a 0.25° × 0.25° spatial resolution are used in this study. The tropospheric NO₂ VCDs are calculated by Stratosphere–troposphere separation (STS) scheme proposed by numerous previous studies (Bucsela et al., 2013; Lamsal et al., 2014; Goldberg et al., 2017). The STS scheme first subtract the stratospheric NO₂ slant column densities (SCDs) from the total NO₂ SCDs and then it divides the resulting tropospheric NO₂ SCDs by the tropospheric air mass factor (AMF). The formulation for calculating tropospheric NO₂ VCDs is as follow:

$$VCD_{trop} = \frac{SCD_{total} - SCD_{strat}}{AMF_{trop}} \quad (1)$$

where AMF is defined as the ratio of the SCD to the VCD (Solomon et al., 1987),

$$AMF_{trop} = \frac{SCD_{trop}}{VCD_{trop}} \quad (2)$$

The tropospheric AMF are calculated by NO₂ profiles simulated by the Global Modeling Initiative (GMI) chemistry transport model with the horizontal resolution of 1° × 1.25° (Rotman et al., 2001). Separation of stratospheric and tropospheric columns is achieved by the local analysis of the stratospheric field over unpolluted areas (Bucsela et al., 2013). The OMI tropospheric NO₂ VCDs dataset has been used in many studies to investigate O₃ formation regime and regional pollution & transport (Lin et al., 2010; Zhang et al., 2017; Duncan et al., 2013; Liu et al., 2016). In this study, only the LV3 data product collected with cloud radiance fractions of less than 30% is used (Streets et al., 2013).

2.1.2 Ground level NO₂ data

We extract ground level NO₂ data over the YRD from the China National Environmental Monitoring Center (CNEMC) network (<http://www.cnemc.cn/en/>, last access: November 26, 2021). The CNEMC network has operated more than 3000 monitoring sites that almost cover all major cities over China by 2020. The CNEMC datasets have been used in many studies for evaluation of regional atmospheric pollution & transport (Li et al., 2021; Lu et al., 2019a; Lu et al., 2020; Sun et al., 2021a; Yin et al., 2021a; Zhao et al., 2016; He et al., 2017). As one of the six key atmospheric pollutants (CO, SO₂, NO₂, PM₁₀, O₃, and PM_{2.5}) routinely measured by the CNEMC network, ground level NO₂ measurements at 188 sites in 40 cities over the YRD are available since 2014. In this study, comparisons between the OMI NO₂ data product and the ground level NO₂ measurements are only performed over 6 key megacities, i.e., Shanghai, Nanjing, Hangzhou, Suzhou, Ningbo, and Hefei, within the YRD. The population, geolocation, the number of measurement site, and data



range of each city are summarized in Table 1. The number of measurement site in each city ranges from 8 to 11, the altitude ranges from 3 to 50 m (above sea level, a.s.l.), and the population ranges from 0.9 to 2.5 million. All ground level NO₂ data at each station are measured by active differential absorption ultraviolet (UV) analyzers. We use a data quality control method following previous studies to remove unreliable NO₂ data (Lu et al., 2019a; Lu et al., 2020; Sun et al., 2021a; Yin et al., 2021a). Specifically, we first convert all hourly measurements into Z scores, we then remove the measurement if its Z score meets one of the following rules: (1) Z_i is larger or smaller than the previous value Z_{i-1} by 9 ($|Z_i - Z_{i-1}| > 9$); (2) The absolute value of Z_i is greater than 4 ($|Z_i| >$
 4); (3) the ratio of the Z value to the third-order center moving average is greater than 2 ($\frac{3Z_i}{Z_{i-1}+Z_i+Z_{i+1}} >$
 2), where i represents the i^{th} hourly measurement data. After removing OUTLIERS with above filter criteria, we finally average NO₂ data at all measurement sites in each city to form a city representative NO₂ dataset.

2.2 Meteorological fields

We obtain meteorological fields during 2005-2020 from the second Modern-Era Retrospective analysis for Research and Applications (MERRA-2) (Gelaro et al., 2017). This dataset is produced by the NASA Global Modeling and Assimilation Office (<https://gmao.gsfc.nasa.gov/reanalysis/MERRA-2/>, last accessed: 1 August, 2021) with a spatial resolution of $0.5^\circ \times 0.625^\circ$, temporal resolutions of 1 h for boundary layer height and surface meteorological variables, and 3 h for other variables. Previous studies have verified that meteorological fields provided by MERRA-2 match well with the meteorological parameters observed by Chinese weather stations (Song et al., 2018; Carvalho, 2019; Wang et al., 2017; Kishore Kumar et al., 2015; Zhou et al., 2017). In order to match OMI observations which are available at about 13:30 LT, the average for meteorological data is only performed between 13:00 and 14:00 LT.

2.3 Multiple linear regression (MLR) model

We establish a multiple linear regression (MLR) model to quantify the contributions of meteorology and anthropogenic emission to the long-term variabilities of tropospheric NO₂ VCDs during 2005-2020 over the YRD. Similar MLR methodologies have been used in previous studies to estimate the contributions of meteorology and emission to the variabilities of O₃ and PM_{2.5} in North America, Europe and China (Li et al., 2019; Li et al., 2020; Xu et al., 2011; Zhai et al., 2019; Zhao and Wang, 2017). The meteorological parameters used in our MLR model are elaborated in Table 2.

In order to highlight the variabilities of tropospheric NO₂ VCDs, we follow the method of previous studies and calculate tropospheric NO₂ VCDs anomalies ($y_{anomaly}$) by subtracting a reference value ($y_{reference}$) from all tropospheric NO₂ observations ($y_{individual}$) (Hakkarainen et al., 2016; Hakkarainen et al., 2019; Mustafa et al., 2021). The formulation of this method is expressed as:

$$y_{anomaly} = y_{individual} - y_{reference} \quad (3)$$

In this study, we take the average of all tropospheric NO₂ VCDs from 2005 to 2020 (i.e., the 16-year mean) as the reference value. The MLR model for each city is explained as:



$$\mathbf{y} = \beta_0 + \sum_{k=1}^{11} \beta_k \mathbf{x}_k \quad (4)$$

where \mathbf{y} are the regression result for monthly OMI tropospheric NO₂ VCDs anomalies, β_0 is the intercept, and \mathbf{x}_k ($k \in [1, 11]$) are the meteorological variables. The regression coefficients β_k are calculated by nonlinear least squares fitting. This MLR model finds the optimal regression result by minimizing the sum of squares of the fitting residual and then solves regression coefficients β_k by the following equation:

$$\beta_k = (\sum \mathbf{x}_k \mathbf{x}_k^T)^{-1} (\sum \mathbf{x}_k \mathbf{y}_k) \quad (5)$$

The regression results \mathbf{y} represent the meteorology induced contributions to the variabilities of tropospheric NO₂ VCDs. Since both soil and lightning NO_x are meteorology dependent, the effects of soil and lightning NO_x on NO₂ variability are also attributed to meteorology contribution. The difference \mathbf{y}' between the monthly OMI tropospheric NO₂ VCDs anomalies $\mathbf{y}_{anomaly}$ and \mathbf{y} calculated as equation (6) represents the portion that cannot be explicitly explained by the meteorological influence.

$$\mathbf{y}' = \mathbf{y}_{anomaly} - \mathbf{y} \quad (6)$$

By subtracting the meteorological influence from the total NO₂ amounts, the \mathbf{y}' is referred to as the aggregate contribution of anthropogenic emission. Positive \mathbf{y} and \mathbf{y}' indicate that meteorology and anthropogenic emission cause tropospheric NO₂ VCDs above the reference value (i.e., the 16-year mean), respectively. In contrast, negative \mathbf{y} and \mathbf{y}' indicate that meteorology and anthropogenic emission cause tropospheric NO₂ VCDs below the reference value, respectively.

Since the meteorological parameters listed in Table 2 differ in units and magnitudes, which could lead to unstable performance of the model. Therefore, we normalized all meteorological parameters via equation (7) before using them in regression. This normalization pre-processing procedure can also speed up the convergence of the MLR model.

$$\mathbf{z}_k = \frac{\mathbf{x}_k - \mathbf{u}_k}{\sigma_k} \quad (7)$$

where \mathbf{u}_k and σ_k are the average and 1 σ standard deviation (STD) of \mathbf{x}_k , and \mathbf{z}_k is the normalized value for parameter \mathbf{x}_k .

3. Temporal-spatial variabilities of tropospheric NO₂ VCDs over the Yangtze River Delta

3.1 Variabilities at provincial level

We present the temporal-spatial distribution of the annual averaged tropospheric NO₂ VCDs over the YRD from 2005 to 2020 in Figure 1. The major pollution areas for tropospheric NO₂ VCDs over the YRD are located in the south of Jiangsu Province and north of Zhejiang Province. In addition, NO₂ pollution in eastern Anhui Province showed an increasing trend during 2005-2013 and became one of the major pollution areas within YRD during 2010-2013. The amplitudes of tropospheric NO₂ VCDs over the YRD showed large year to year variabilities from 2005 to 2020 but spatial extensions of the major pollution areas are almost constant over years. Among all the pollution areas, the heaviest pollution regions are uniformly located in the densely populated and highly industrialized megacities such as Shanghai, Nanjing, Suzhou, Hangzhou, Ningbo, and Hefei.

The annual means and seasonal cycles of tropospheric NO₂ VCDs over the YRD during 2005-2020 at Province or municipality level, i.e., Anhui Province, Jiangsu Province, Zhejiang Province, and Shanghai municipality, are presented in Figure 2. Tropospheric NO₂ VCDs over each province are calculated by averaging all observations within the boundary of each province. For seasonal



variability, clear seasonal features over the whole YRD region and each province are observed (Figure 2a): (1) high levels of tropospheric NO_2 VCDs occur in late winter to spring and low levels of tropospheric NO_2 VCDs occur in later summer to autumn; (2) the 1σ STDs in late winter to spring are larger than those in later summer to autumn; and (3) seasonal cycles of tropospheric NO_2 VCDs over Jiangsu, Zhejiang and the whole YRD region show bimodal patterns, i.e., two seasonal peaks occur around March and December or January, and one seasonal trough occurs around September; but these over Anhui shows a unimodal pattern and don't have the peak around March. The tropospheric NO_2 VCDs present a maximum monthly mean value of (1.93 ± 0.21) , (2.40 ± 0.25) , (1.61 ± 0.16) , and $(1.91 \pm 0.16) \times 10^{16}$ molecules/ cm^2 in January or December over Anhui, Jiangsu, Zhejiang, and the whole YRD region, respectively. The minimum monthly mean values over Anhui, Jiangsu, Zhejiang and the whole YRD region occur in July, with values of (0.35 ± 0.05) , (0.83 ± 0.07) , (0.57 ± 0.06) , and $(0.39 \pm 0.01) \times 10^{16}$ molecules/ cm^2 , respectively.

Except a few anomalies such as the year-to-year decrease in 2005-2006, and the increases in 2016-2017 and 2018-2019, the overall inter annual variabilities of tropospheric NO_2 VCDs over the YRD can be divided into two stages (Fig. 2b). The first stage was from 2005 to 2011, which showed overall increasing trends in tropospheric NO_2 VCDs over the YRD. During 2005 to 2009 of this stage, change rates of tropospheric NO_2 VCDs were less pronounced, where the 2009 relative to 2005 levels have only increased by $(0.33 \pm 0.02) \times 10^{15}$ $(3.96 \pm 0.25) \%$, $(1.05 \pm 0.11) \times 10^{15}$ $(8.55 \pm 0.08) \%$, and $(0.46 \pm 0.03) \times 10^{15}$ molecule/ m^2 $(5.05 \pm 0.32) \%$ over Anhui, Jiangsu and the whole YRD region, respectively, and leveled off over Zhejiang. However, tropospheric NO_2 VCDs in 2011 relative to 2009 showed significantly increments of $(2.88 \pm 0.23) \times 10^{15}$ $(33.78 \pm 2.70) \%$, $(3.81 \pm 0.32) \times 10^{15}$ $(29.01 \pm 2.45) \%$, $(2.08 \pm 0.18) \times 10^{15}$ $(27.97 \pm 2.43) \%$, $(2.10 \pm 0.19) \times 10^{15}$ molecule/ m^2 $(21.59 \pm 1.95) \%$ over Anhui, Jiangsu, Zhejiang and the whole YRD region, respectively. The second stage was from 2011 to 2020, which showed overall decreasing trends in tropospheric NO_2 VCDs over the YRD. The total decrements over Anhui, Jiangsu, Zhejiang and the whole YRD region in 2020 relative to 2011 are $(4.91 \pm 0.39) \times 10^{15}$ $(41.48 \pm 3.30) \%$, $(4.82 \pm 0.31) \times 10^{15}$ $(43.25 \pm 2.72) \%$, $(3.78 \pm 0.36) \times 10^{15}$ $(40.47 \pm 4.12) \%$, $(4.91 \pm 0.39) \times 10^{15}$ molecule/ m^2 $(41.48 \pm 3.30) \%$, respectively.

We have followed the methodology of (Li et al., 2020)) and used the linear regression model to estimate the inter annual trends of tropospheric NO_2 VCDs over the YRD (Table 3). During 2005-2011, inter annual trends of tropospheric NO_2 VCDs over the YRD region and each province spanned a wide range of $(1.74 \pm 0.72) \times 10^{14}$ molecules/ $\text{cm}^2 \cdot \text{yr}^{-1}$ ($p=0.02$) to $(5.94 \pm 1.01) \times 10^{14}$ molecules/ $\text{cm}^2 \cdot \text{yr}^{-1}$ ($p<0.01$), indicating a regional representative of each dataset. In contrast, inter annual trends of tropospheric NO_2 VCDs over the YRD region and each province from 2011 to 2020 varied over (-4.86 ± 0.49) to $(-8.16 \pm 0.82) \times 10^{14}$ molecules/ $\text{cm}^2 \cdot \text{yr}^{-1}$ ($p<0.01$). For the aggregate trends during 2005-2020, tropospheric NO_2 VCDs over the whole YRD region and each province are negative. The largest and lowest decreasing trends are observed in Jiangsu and Anhui, with values of $(-1.92 \pm 0.30) \times 10^{14}$ molecules/ $\text{cm}^2 \cdot \text{yr}^{-1}$ ($p<0.01$) and $(-0.92 \pm 0.26) \times 10^{14}$ molecules/ $\text{cm}^2 \cdot \text{yr}^{-1}$ ($p<0.01$), respectively.

3.2 Variabilities at megacity level

The annual means and seasonal cycles of tropospheric NO_2 VCDs over the major megacities within YRD during 2005-2020 are presented in Figure 3. Similar to the derivation of provincial level NO_2 , tropospheric NO_2 VCDs over each megacity are calculated by averaging all observations



within the boundary of each megacity. The results show that the amplitudes and variabilities of tropospheric NO₂ VCDs at megacity level are basically coincident with those at the corresponding provincial levels. Overall, the amplitudes and 1σ STDs of NO₂ seasonal cycles in cold seasons are larger than those in warm seasons, and the inter annual NO₂ variabilities at megacity level can also be divided into two stages, i.e., an overall increasing stage during 2005-2011 and a decreasing stage during 2011-2020. As a result, it is feasible to select these major megacities as representatives for mapping the drivers of NO₂ variabilities over the YRD.

Specifically, megacity level of tropospheric NO₂ VCDs show seasonal maxima in December and seasonal minima in July. Seasonal maxima over Hefei, Shanghai, Nanjing, Suzhou, Hangzhou, and Ningbo are (2.03 ± 0.15) , (2.80 ± 0.23) , (2.62 ± 0.25) , (2.66 ± 0.16) , (1.83 ± 0.18) , and $(2.27 \pm 0.21) \times 10^{16}$ molecules/cm², and seasonal minima are (0.34 ± 0.04) , (0.83 ± 0.11) , (0.58 ± 0.06) , (0.62 ± 0.05) , (0.32 ± 0.02) , and $(0.38 \pm 0.03) \times 10^{16}$ molecules/cm², respectively. The seasonal maxima are on average (82.27 ± 2.34) %, (67.19 ± 1.56) %, (71.06 ± 2.32) %, (83.33 ± 3.05) %, (77.62 ± 2.89) %, and (70.84 ± 2.76) % higher than the seasonal minima over respective megacity. As commonly observed, the seasonal variability of tropospheric NO₂ VCDs with respect to their annual means spanned a wide range of -55.1% to 103.5% depending on season and measurement time (Figure 3a).

Tropospheric NO₂ VCDs in all megacities show the maximum values in 2011, where the maximum values over Hefei, Shanghai, Suzhou, Ningbo, Nanjing and Hangzhou are (1.41 ± 0.25) , (2.18 ± 0.23) , (1.81 ± 0.17) , (1.39 ± 0.12) , (1.88 ± 0.18) and $(1.19 \pm 0.14) \times 10^{16}$ molecules/cm², respectively (Figure 3b). In terms of the increments relative to the 2005 levels, Hefei and Shanghai from 2005 to 2011 have the largest and lowest increments of $(5.37 \pm 0.51) \times 10^{15}$ molecules/cm² (61.77 ± 5.87) % and $(2.62 \pm 0.27) \times 10^{15}$ molecules /cm² (14.68 ± 1.51) %, respectively. The increments over other cities varied over $(3.31 \pm 0.32) \times 10^{15}$ molecules /cm² (31.20 ± 3.02) % to $(5.21 \pm 0.41) \times 10^{15}$ molecules/cm² (38.40 ± 3.02) %. In terms of the decrements relative to the 2011 levels, Shanghai and Hangzhou from 2011 to 2020 have the largest and lowest decrements of $(9.77 \pm 0.82) \times 10^{15}$ molecules/cm² (46.89 ± 3.94) and $(5.28 \pm 0.45) \times 10^{15}$ molecules/cm² (45.43 ± 3.87) %, respectively. The decrements over other cities are also evident and varied over $(6.33 \pm 0.58) \times 10^{15}$ molecules/cm² (45.53 ± 4.18) % to $(9.05 \pm 0.98) \times 10^{15}$ molecules/cm² (48.12 ± 5.21) %. A few anomalies are also observed in some megacities and are in good agreement with the corresponding provincial levels. For example, tropospheric NO₂ VCDs over Hefei and Suzhou had increased by $(0.09 \pm 0.01) \times 10^{15}$ molecules/cm² (0.77 ± 0.09) % and $(0.80 \pm 0.07) \times 10^{15}$ molecules/cm² (4.90 ± 0.43) % in 2013 relative to 2012 levels, respectively. In addition, tropospheric NO₂ VCDs over Hefei, Shanghai, Nanjing, Hangzhou, and Suzhou had increased by $(0.65 \pm 0.12) \times 10^{15}$ (8.41 ± 1.55) %, $(0.35 \pm 0.02) \times 10^{15}$ (2.66 ± 0.15) %, $(0.86 \pm 0.18) \times 10^{15}$ (8.16 ± 1.71) %, $(0.55 \pm 0.08) \times 10^{15}$ (8.68 ± 1.26) %, and $(0.29 \pm 0.05) \times 10^{15}$ molecules/cm² (2.52 ± 0.43) % in 2019 relative to 2018 levels, respectively.

The inter annual trends of tropospheric NO₂ VCDs during 2005-2011 over all cities are positive and span a wide range of (1.91 ± 1.50) to $(6.70 \pm 0.10) \times 10^{14}$ molecules/cm²·yr⁻¹ ($p < 0.01$) (Table 4). In contrast, the inter annual trends of tropospheric NO₂ VCDs during 2011-2020 over all cities are negative. The largest and lowest decreasing trends are observed in Nanjing and Hangzhou, with values of (-11.01 ± 0.90) and $(-6.31 \pm 0.71) \times 10^{14}$ molecules/cm²·yr⁻¹ ($p < 0.01$), respectively. For the aggregate trends during 2005-2020, tropospheric NO₂ VCDs over all cities are negative. The largest and lowest decreasing trends are observed in Shanghai and Hefei, with values of $(-4.58 \pm 0.43) \times 10^{14}$



333 molecules/cm²·yr⁻¹ ($p < 0.01$) and $(-0.30 \pm 3.43) \times 10^{14}$ molecules/cm²·yr⁻¹ ($p = 0.385$), respectively.

334 3.3 Comparisons with the CNMEC data

335 In order to investigate if satellite column measurements can represent the near surface
336 variabilities, we have compared the OMI tropospheric NO₂ VCDs data over the 6 megacities within
337 the YRD with the ground level NO₂ data provided by the CNMEC (Figure 4). The comparisons over
338 all megacities were performed on monthly basis between June 2014 and December 2020. For each
339 city, the CNMEC ground level NO₂ measurements nearest to the OMI ground grid were included
340 for comparison. Considering the overpass time of OMI is at about 13:30 LT, we only average the
341 ground level NO₂ data between 13:00 and 14:00 LT for comparison, which ensures that the temporal
342 differences between the CNMEC and OMI dataset are all within ± 30 minutes. With these rules,
343 there are over 700 matching samples in each city available for comparison.

344 Correlation plots of OMI tropospheric NO₂ VCDs data against the CNMEC ground level NO₂
345 measurements are shown in Figure 4. The results show that the NO₂ variabilities observed by OMI
346 and the CNMEC are in good agreements over all megacities, with correlation coefficients (r^2) of
347 0.88, 0.81, 0.89, 0.88, 0.86 and 0.83 for Hangzhou, Hefei, Nanjing, Ningbo, Shanghai, and Suzhou,
348 respectively. The discrepancies between OMI and CNMEC data can be mainly attributed to their
349 differences in temporal-spatial resolutions. OMI averages NO₂ concentration at about 13:30 LT over
350 a large coverage due to its relatively coarse spatial resolution (Wallace and Kanaroglou, 2009; Zheng
351 et al., 2014). The CNMEC data represent the averaged point concentrations between 13:00 and
352 14:00 LT around the measurement site. NO₂ is a short lifetime species and characterized by large
353 temporal-spatial variabilities. Any temporal-spatial inhomogeneity in NO₂ concentration could
354 affect the comparison (Meng et al., 2010; Wallace and Kanaroglou, 2009). Considering above
355 differences, the correlations of the two datasets over all megacities are satisfactory. The tropospheric
356 NO₂ column measurements can be used as representatives of near-surface conditions. As a result,
357 to simplify calculations, we only use ground-level meteorological data for MLR regression.

358 Over polluted atmosphere, the NO₂ column measurements can be used as representative of
359 near-surface conditions because tropospheric NO₂ has a vertical distribution that is heavily weighted
360 toward the surface (Kharol et al., 2015; Zhang et al., 2017; Duncan et al., 2016; Duncan et al.,
361 2013; Kramer et al., 2008). Many studies have taken advantage of this favourable vertical
362 distribution of NO₂ to derive surface emissions of NO₂ from space (Silvern et al., 2019; Boersma et
363 al., 2009; Streets et al., 2013; Anand and Monks, 2017; Lu et al., 2015; Ghude et al., 2013; Cooper et
364 al., 2020). Meanwhile, the use of NO₂ column measurements to explore tropospheric O₃ sensitivities
365 has been the subject of several past studies, which disclosed that this diagnosis of O₃ production
366 rate (PO₃) is consistent with the findings of surface photochemistry (Jin et al., 2017; Jin and
367 Holloway, 2015; Sun et al., 2018; Yin et al., 2021b; Sourì et al., 2017; Sun et al., 2021b; Jin et al.,
368 2020; Choi and Sourì, 2015; Schroeder et al., 2017; Baruah et al., 2021).

369 4 Implications and drivers

370 We incorporate the 11 meteorological parameters listed in Table 2 into the MLR model to fit
371 the time series of monthly averaged tropospheric NO₂ VCDs from 2005 to 2020 over the 6
372 megacities within the YRD (Figure S1). Correlation plots of the MLR regression results and the
373 satellite tropospheric NO₂ data are shown in Figure 5. The results show that the MLR model can



well reproduce the seasonal variabilities of tropospheric NO₂ VCDs over each city with correlation coefficients of 0.85 to 0.90. We separate the contributions of meteorology and anthropogenic emission to the NO₂ variability over the 6 megacities with the methodology described in section 2.3. Figure 6 shows monthly averaged tropospheric NO₂ VCDs along with the meteorological-driven contributions and the anthropogenic-driven contributions in each city. Figure 7 is the same as Figure 6, but the statistics are based on annual average.

4.1 Drivers of seasonal cycles of tropospheric NO₂ VCDs

As shown in Figure 6 for all megacities, the seasonal variabilities of meteorological contributions are consistent with those of tropospheric NO₂ VCDs except the period from February to March, and the anthropogenic contributions varied around zero throughout the year except in December and February. This means that the seasonal variabilities of tropospheric NO₂ over the YRD are mainly determined by meteorology (81.01% - 83.91%) and also influenced by anthropogenic emission in December and February. Meteorological contributions are larger than zero in winter and lower than zero in summer, indicating that meteorology increases NO₂ level in winter and decreases NO₂ level in summer. This contrast in meteorological contribution is associated with the seasonal cycle of temperature. Similarly, anthropogenic contributions are larger than zero in December and lower than zero in February, representing anthropogenic emission increases NO₂ level in December and decreases NO₂ level in February. The enhanced anthropogenic contributions in December are mainly attributed to more extensive anthropogenic activities such as residential heating in megacities in this period which usually results in more anthropogenic NO₂ emissions due to the increase in energy and fuel consumptions. The decreased anthropogenic contributions in February are attributed to the Spring Festival. We elaborate the analysis as bellow.

As shown in Figure S2, the vast majorities of meteorological contributions over all megacities are from temperature and additional minor contributions over some cities such as Nanjing, Shanghai, and Suzhou are attributed to relative humidity. Significant negative correlations between temperature and tropospheric NO₂ VCDs are observed in all megacities (Figure S3, Table 5). Higher temperature tends to decrease tropospheric NO₂ VCDs and vice versa. This is because higher temperature conditions could accelerate the chemical reaction that destructs NO₂ in the troposphere (Pearce et al., 2011; Yin et al., 2021a). Surface pressure and relative humidity have high positive and negative correlations with tropospheric NO₂ VCDs, respectively, but their contribution levels are much lower than the temperature. All other meteorological variables only have weak correlations with tropospheric NO₂ VCDs (Table 5).

In all cities except Hefei, there is a significant increase in NO₂ level from February to March. The maximum and minimum increments occur in Shanghai and Nanjing, with values of $(3.28 \pm 0.29) \times 10^{15}$ molecules/cm² (16.37 ± 1.45) % and $(0.47 \pm 0.05) \times 10^{15}$ molecules/cm² (2.60 ± 0.28) %, respectively. In contrast, the meteorological contributions show decreased change rates in the same period. As a result, this increase in NO₂ level from February to March could be attributed to anthropogenic emission rather than meteorology. Indeed, anthropogenic contributions show significant increases of (3.95 ± 0.32) to $(6.53 \pm 0.55) \times 10^{15}$ molecules/cm² over all megacities from February to March. The most important festival in China-the Spring Festival-typically occurs in February, when a large number of migrants in megacities return to their hometowns for holiday and most industrial productions are shut down, which could cause significant reductions in anthropogenic emission. In March, these migrants get back to work and all industrial enterprises



resumed productions, which could cause a rebound in anthropogenic emission. The seasonal maxima of NO_2 in March are not observed in Hefei is because the anthropogenic emission induced increases are offset by meteorology induced decreases.

2020 is a special year compared to all other years, when a large-scale lockdown occurred in February and some regional travel restrictions occasionally occurred in other seasons across China due to COVID-19 disease. In the comparison, we removed all NO_2 measurements in 2020 to eliminate the influence of COVID-19. The monthly averaged tropospheric NO_2 VCDs from 2005 to 2019 along with the meteorological contributions and the anthropogenic contributions in each city are shown in Figure S4. We obtained the same conclusion as that from Figure 6, indicating the drivers of seasonal cycles of tropospheric NO_2 VCDs deduced above are consistent over years.

4.2 Drivers of inter annual variabilities of tropospheric NO_2 VCDs

As shown in Figure 7 for all megacities, the inter annual variabilities of anthropogenic contributions are in good agreement with those of tropospheric NO_2 VCDs, indicating inter annual variabilities of tropospheric NO_2 VCDs are mainly driven by anthropogenic emission. The same as those of tropospheric NO_2 VCDs, the inter annual anthropogenic contributions over each city can also be divided into two stages, i.e., an overall increasing stage during 2005–2011 and a decreasing stage during 2011–2020. For the first stage (2005–2011), anthropogenic contributions account for 84.72%, 92.96%, 93.52%, 79.06%, 97.12%, and 90.21% of the increases in tropospheric NO_2 VCDs, while meteorological contributions account for 15.28%, 7.04%, 6.48%, 20.94%, 2.88%, and 9.79% over Hangzhou, Hefei, Nanjing, Ningbo, Shanghai, and Suzhou, respectively. The annual averaged meteorological contributions over each city varied around zero in all years except few anomalies in some years. For example, meteorological contributions over all cities are larger than zero in 2005 and 2011 but lower than zero after 2014. Pronounced anomalies include the enhancements occurred in 2011 in all cities and the decrements in 2015 over Suzhou, in 2018 over Hangzhou, and in 2016 over other cities. All these anomalies in meteorological contributions are highly correlated with temperature anomalies (Figure S5). As shown in Figure S6, the temperature in all cities is lower than the reference value (i.e., the 16-year mean) in 2005 and 2011 and larger than the reference value after 2014. As a result, in addition to anthropogenic emission, the NO_2 enhancements in 2011 are partly attributed to the lower temperature in this year. Meanwhile, higher temperature in YRD region in recent years favors the decrease in tropospheric NO_2 VCDs. For the second stage (2011–2020), anthropogenic contributions account for 70.15 %, 65.22 %, 66.97 %, 73.45 %, 74.43 %, and 73.84 % of the decreases in tropospheric NO_2 VCDs, while meteorological contributions account for 29.85%, 34.78%, 33.03 %, 26.55 %, 25.57 %, and 26.16 % over Hangzhou, Hefei, Nanjing, Ningbo, Shanghai, and Suzhou, respectively.

Since anthropogenic NO_2 emissions are highly related to economic and industrial activities (Lin and McElroy, 2011; Russell et al., 2012; Vrekoussis et al., 2013; Guerriero et al., 2016), to understand the inter annual variabilities of tropospheric NO_2 VCDs, we have investigated the inter annual variabilities of Gross Domestic Product (GDP) over the YRD from primary sector, secondary sector and tertiary sector (<http://www.stats.gov.cn/>, last accessed: 1 August, 2021) from 2005 to 2020. The primary sector includes agriculture, forestry, animal husbandry, and fishery; The secondary industry includes mining, manufacturing, power, heat, gas and water production and supply, and construction; The tertiary industry, namely the service industry, refers to all industries



excluded the primary industry and the secondary industry. The secondary industry is more related to energy and fuel consumptions, and it thus dominates the anthropogenic NO_2 emissions. Figure S7 shows the time series of GDP over the YRD from 2005 to 2020 and Figure 8 is the same as Figure S7 but for year-to-year increment, i.e., the increase in GDP at a given year relative to its previous year. The results show that the GDP of each province within the YRD increased over time starting from 2005 but the relative contribution of each industry sector is different from year to year. The primary sector-related GDP is relative constant, but both the secondary sector and tertiary sector related GDPs show significant increasing trends from 2005 to 2020.

During 2009 to 2011, the GDPs have increased significantly by 198.45, 483.86, 656.40, and 327.05 billion yuan over Shanghai, Zhejiang, Jiangsu, and Anhui, where the secondary sector contributions account for 46.50%, 53.64%, 48.99%, and 60.34% respectively. Before 2011, much of China's economic growths still rely on the high-carbon fossil energy system and efforts to control atmospheric pollution were relatively small. These significant increases in GDP could cause significant increases in anthropogenic NO_2 emissions. After 2011, China has implemented a series of clean air measures to tackle air pollution across China. These measures include the reduction of industrial pollutant emissions, the adjustment of industrial structure and energy mix, and other compulsive policies (China State Council, 2013). Zheng et al. (2018a) have estimated China's anthropogenic emission trends from 2010 to 2017 with the bottom-up emission inventory. Zheng et al. (2018a) found that, as the consequence of clean air measures, anthropogenic NO_x emissions across China during 2010–2017 have been decreased by 17%.

Although the total GDPs over all megacities are still increasing over time after 2011, much of these increases are from the tertiary sector, indicating the effectiveness of the adjustment of industrial structure and energy mix. The largest anthropogenic NO_2 producer from the tertiary sector is attributed to the transportation industry including such as traffic and cargo transport, etc. Chinese government had implemented stringent restrictions on vehicle exhaust emissions after 2011 (Ministry of Ecology and Environment of the People's Republic of China, 2016, 2011). For example, Chinese government implemented the fourth and the fifth national motor vehicle pollutant emissions standards in 2011 and 2018, respectively, which mandate 30% and 60% reductions in vehicle NO_x emissions relative to the third national standard (Ministry of Ecology and Environment of the People's Republic of China, 2007, 2018). These stringent measures could significantly reduce anthropogenic NO_2 emissions from the tertiary sector. Overall, the decreasing trends in tropospheric NO_2 VCDs from 2011 to 2020 over all megacities within the YRD are mainly attributed to the stringent clean air measures in this period which either adjust high energy industrial structure toward low energy industrial structure or directly reduce pollutant emissions from different industrial sectors.

5 Conclusions

In this study, we have quantified the long-term variabilities and the underlying drivers of tropospheric NO_2 VCDs from 2005–2020 over the Yangtze River Delta (YRD) by OMI LV3 NO_2 data product and MLR regressions. The major pollution areas for tropospheric NO_2 VCDs over the YRD are located in the south of Jiangsu Province and north of Zhejiang Province. In addition, NO_2 pollution in eastern Anhui Province showed an increasing trend during 2005–2013 and became one of the major pollution areas within YRD during 2010–2013. The amplitudes of tropospheric NO_2



VCDs over the YRD showed large year to year variabilities from 2005 to 2020 but spatial extensions of the major pollution areas are almost constant over years. Among all the pollution areas, the heaviest pollution regions are uniformly located in the densely populated and highly industrialized megacities such as Shanghai, Nanjing, Suzhou, Hangzhou, Ningbo, and Hefei. For six megacities the space borne tropospheric results have been compared to surface in-situ data, yielding correlation coefficients between 0.8 and 0.9.

Clear seasonal features and inter annual variabilities of tropospheric NO₂ VCDs over the YRD region are observed. Overall, the amplitudes and 1 σ STDs of NO₂ seasonal cycles in cold seasons are larger than those in warm seasons, and the inter annual NO₂ variabilities at megacity level can be divided into two stages, i.e., an overall increasing stage during 2005-2011 and a decreasing stage during 2011-2020. We have used the MLR regressions to quantify the drivers of tropospheric NO₂ VCDs from 2005 to 2020 over all megacities within the YRD. The seasonal cycles of tropospheric NO₂ VCDs over the YRD are mainly driven by meteorology (81.01% - 83.91%) except in winter when anthropogenic emission contributions are also pronounced (16.09% - 18.99%). The inter annual variabilities of tropospheric NO₂ VCDs are mainly driven by anthropogenic emission (69.18% - 81.34%) except in few years such as 2018 which are partly attributed to meteorology anomalies (39.07% - 91.51%).

The increasing trends in tropospheric NO₂ VCDs from 2005 to 2011 over the YRD are mainly attributed to high energy consumption associated with rapid economic growth which cause significant increases in anthropogenic NO₂ emissions. The decreasing trends in tropospheric NO₂ VCDs from 2011 to 2020 over the YRD are mainly attributed to the stringent clean air measures in this period which either adjust high energy industrial structure toward low energy industrial structure or directly reduce pollutant emissions from different industrial sectors. This study can not only have improved our knowledge with respect to long term evolutions of economic and social development, anthropogenic emission, and the effectiveness of pollution control measures over the YRD, but also have positive implications for forming future clean air policies in the important region.

Code and data availability. Surface NO₂ measurements over the YRD are from <http://www.cnemc.cn/en/>. The OMI LV3 tropospheric NO₂ satellite data can be obtained from https://acdisc.gesdisc.eosdis.nasa.gov/data/Aura_OMI_Level3/. The Chinese economic data can be obtained from <http://www.stats.gov.cn/>. All other data are available on request of the corresponding author (Youwen Sun, ywsun@aiofm.ac.cn).

Author contributions. HY designed the study and wrote the paper. YS supervised and revised this paper. JN, MP, and CL provided constructive comments.

Competing interests. None.

Acknowledgements. This work is jointly supported by the National Key Research and Development Program of China (No.2019YFC0214802), the Youth Innovation Promotion Association, CAS (No.2019434), and the Sino-German Mobility programme (M-0036).



Table 1. Geolocation, the number of measurement site, and population for the 6 megacities within the YRD. Population statistics are based on the seventh nationwide population census in 2020 provided by National Bureau of Statistics of China.

City	Latitude	Longitude	Number of sites	Altitude (m)	Population (million)
Hangzhou	30.29	120.15	11	41.7	1.19
Hefei	31.85	117.25	10	29.8	0.94
Ningbo	29.87	121.55	9	5.1	0.94
Nanjing	32.04	118.77	9	8.9	0.93
Shanghai	31.23	121.47	10	4.5	2.49
Suzhou	31.30	120.62	8	3.5	1.28

Table 2. Meteorological parameters used in the MLR model.

Parameters	Description
T _{2m}	2m air temperature
U _{10m}	10m zonal wind
V _{10m}	10m meridional wind
PBLH	Planetary boundary layer height
TCC	Total cloud area fraction
Rain	Rainfall
SLP	Sea level pressure
SWGDN	Surface incoming shortwave flux
RH _{2m}	2m Relative humidity
TROPH	Tropospheric layer Height

Table 3. Inter annual trends of tropospheric NO₂ VCDs over each province within the YRD and the whole YRD region during 2005 to 2011, 2011 to 2020 and 2005 to 2020.

Province	Annual trend (10 ¹⁴ molecule/m ²)		
	2005-2011	2011-2020	2005-2020
YRD	3.69 ± 0.78 (p<0.01)	-6.18 ± 0.52 (p<0.01)	-1.54 ± 0.23 (p<0.01)
Anhui	4.40 ± 0.89 (p<0.01)	-5.93 ± 0.58 (p<0.01)	-0.92 ± 0.26 (p<0.01)
Jiangsu	5.94 ± 1.01 (p<0.01)	-8.16 ± 0.82 (p<0.01)	-1.92 ± 0.30 (p<0.01)
Zhejiang	1.74 ± 0.72 (p=0.02)	-4.86 ± 0.49 (p<0.01)	-1.41 ± 0.22 (p<0.01)

Table 4. Inter annual trends of tropospheric NO₂ VCDs over each city within the YRD during 2005 to 2011, 2011 to 2020 and 2005 to 2020.

Province	Annual trend (10 ¹⁴ molecule/m ²)		
	2005-2011	2011-2020	2005-2020
Hangzhou	4.07 ± 1.03 (p<0.01)	-6.31 ± 0.71 (p<0.01)	-1.41 ± 0.30 (p<0.01)
Hefei	6.70 ± 0.11 (p<0.01)	-6.73 ± 0.78 (p<0.01)	-0.30 ± 3.43 (p=0.385)
Nanjing	6.50 ± 1.25 (p<0.01)	-11.01 ± 0.90 (p<0.01)	-2.19 ± 0.39 (p<0.01)
Ningbo	3.79 ± 1.16 (p<0.01)	-7.16 ± 0.81 (p<0.01)	-2.51 ± 0.35 (p<0.01)
Shanghai	1.91 ± 1.50 (p=0.204)	-9.91 ± 0.97 (p<0.01)	-4.58 ± 0.43 (p<0.01)
Suzhou	5.84 ± 0.12 (p<0.01)	-7.16 ± 0.81 (p<0.01)	-2.32 ± 0.35 (p<0.01)



Table 5. Correlations of monthly averaged observations against each meteorological parameter from 2005 to 2020.

City	Correlations									
	T _{2m}	U _{10m}	V _{10m}	PBLH	TCC	Rain	SLP	SWGDN	RH _{2m}	TROPH
Hangzhou	-0.81	-0.11	-0.40	-0.43	-0.63	-0.34	0.84	-0.51	-0.78	0.28
Hefei	-0.84	0.02	-0.48	-0.51	-0.57	-0.39	0.83	-0.69	-0.77	0.25
Nanjing	-0.86	0.07	-0.47	-0.45	-0.56	-0.59	0.86	-0.63	-0.83	0.38
Ningbo	-0.84	0.39	-0.71	-0.14	-0.70	-0.47	0.86	-0.54	-0.82	0.07
Shanghai	-0.82	0.59	-0.65	0.08	-0.66	-0.45	0.83	-0.56	-0.83	0.32
Suzhou	-0.87	0.35	-0.59	-0.60	-0.67	-0.59	0.87	-0.72	-0.82	0.45

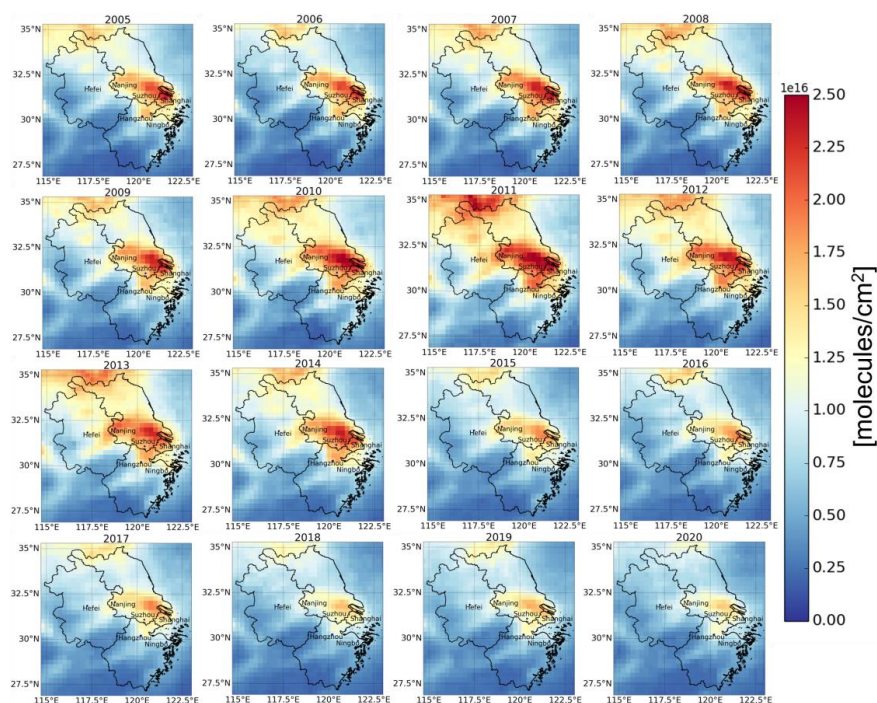


Figure 1. Temporal-spatial variabilities of tropospheric NO₂ VCDs provided by OMI satellite over the YRD from 2005 to 2020. The three provinces (Anhui, Jiangsu, Zhejiang) and six key megacities (Hefei, Nanjing, Suzhou, Shanghai, Hangzhou, Ningbo) are marked.

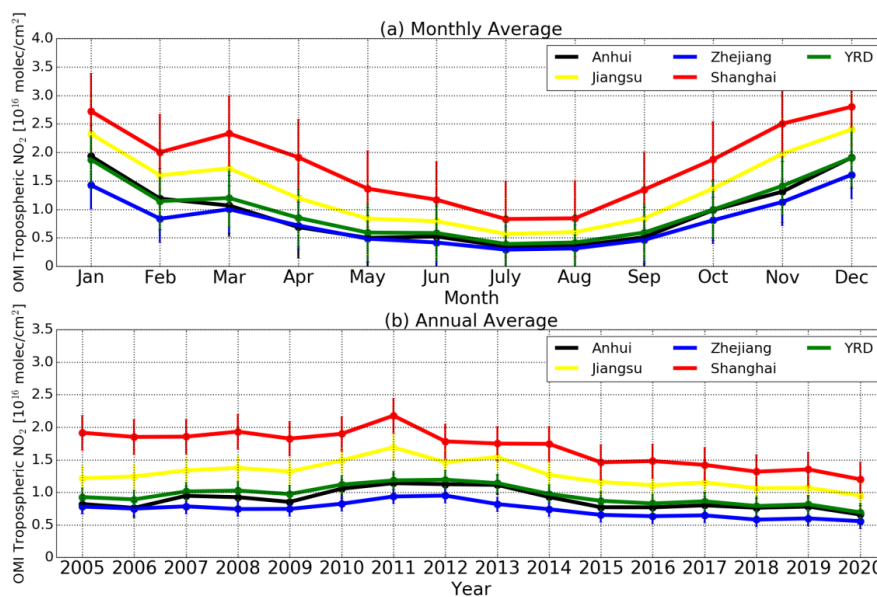


Figure 2. (a) Monthly averaged tropospheric NO₂ VCDs over the whole YRD region (green dots and lines), Anhui Province (black dots and lines), Zhejiang Province (blue dots and lines), and Jiangsu Province (yellow dots and lines). (b) Same as (a) but for annual average. The vertical error bar is 1σ standard variation (STD) within that month or year.

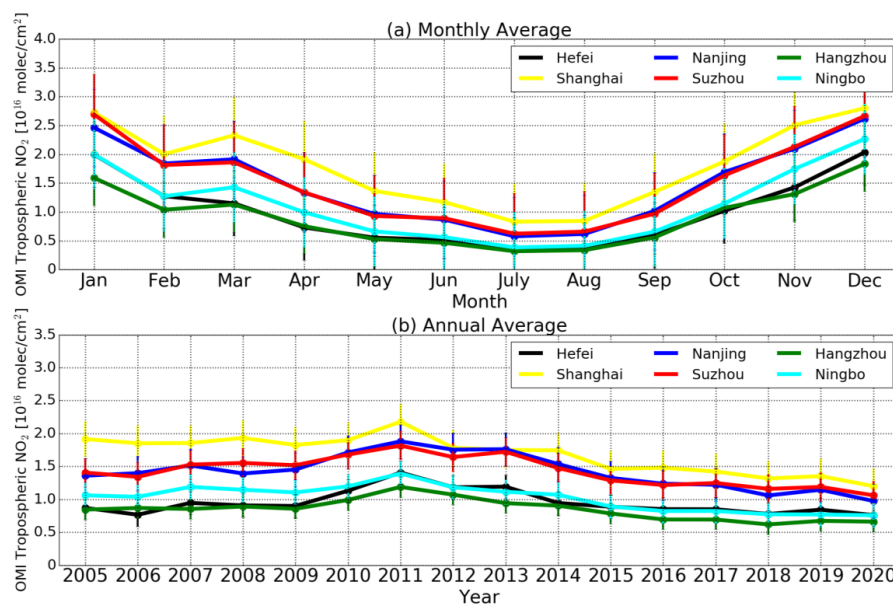
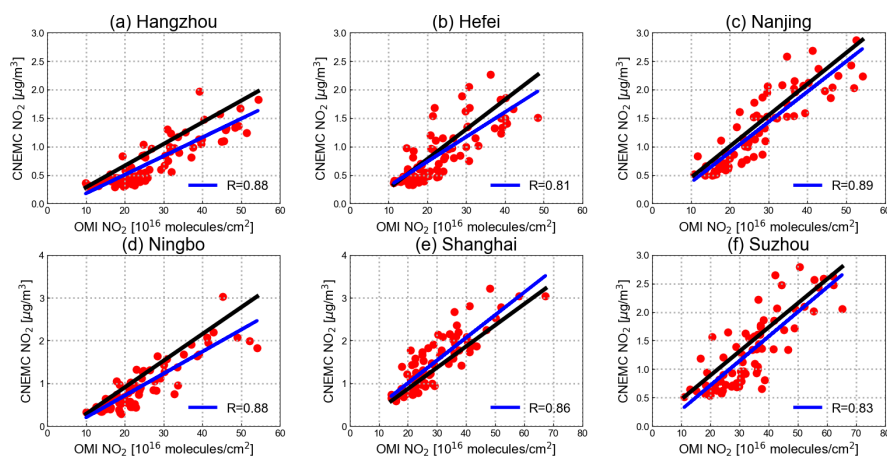


Figure 3. (a) Monthly averaged tropospheric NO₂ VCDs over Hefei (black dots and lines), Nanjing (blue dots and lines), Shanghai (yellow dots and lines), Suzhou (red dots and lines), Hangzhou (green dots and lines), and Ningbo (cyan dots and lines). (b) Same as (a) but for annual average. The vertical error bar is 1 σ standard variation within that month or year.



573

574 **Figure 4.** Correlation of OMI tropospheric NO₂ VCDs against ground-level observations data over
 575 Hefei, Nanjing, Shanghai, Suzhou, Hangzhou and Ningbo. We fitted both datasets directly without
 576 uniform their units, which does not affect the investigation with respect to the agreement of the two
 577 datasets in terms of variabilities. Blue lines are linear fitted lines and black lines are one to one line.
 578

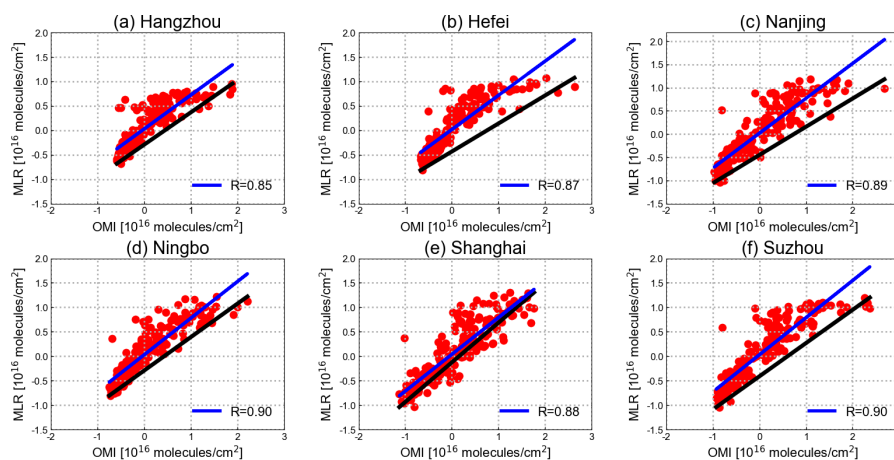


Figure 5. Correlations of OMI tropospheric NO₂ VCDs against the MLR model results over Hefei, Nanjing, Shanghai, Suzhou, Hangzhou, and Ningbo. Blue lines are linear fitted lines and black lines are one to one line.

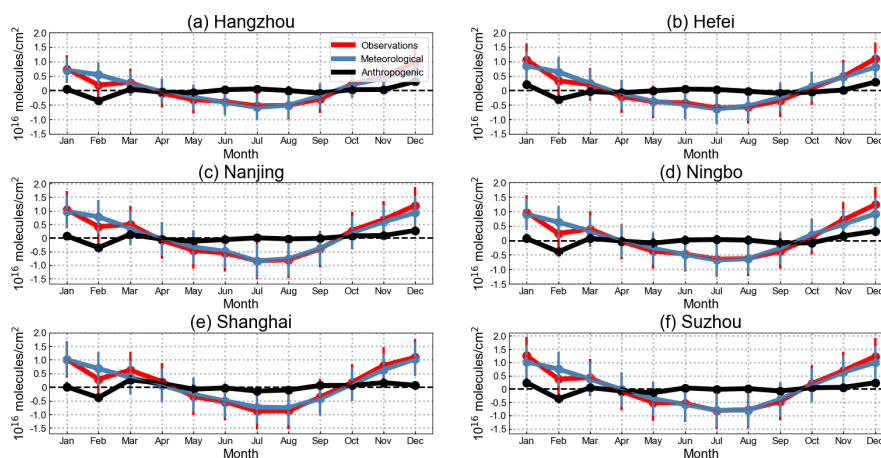


Figure 6. Monthly averaged tropospheric NO₂ VCDs (red dots and lines) along with the meteorological-driven portions (blue dots and lines) and the anthropogenic-driven portions (black dots and lines) over each city within the YRD. The vertical error bar is 1σ standard variation (STD) within that month.

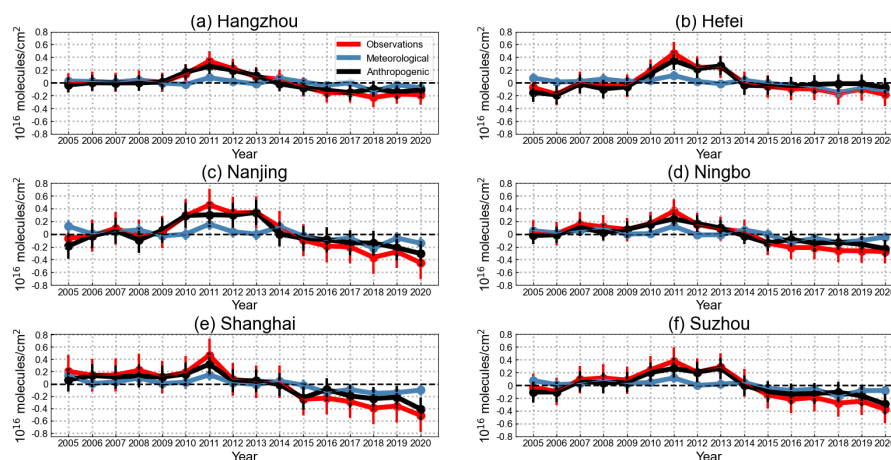
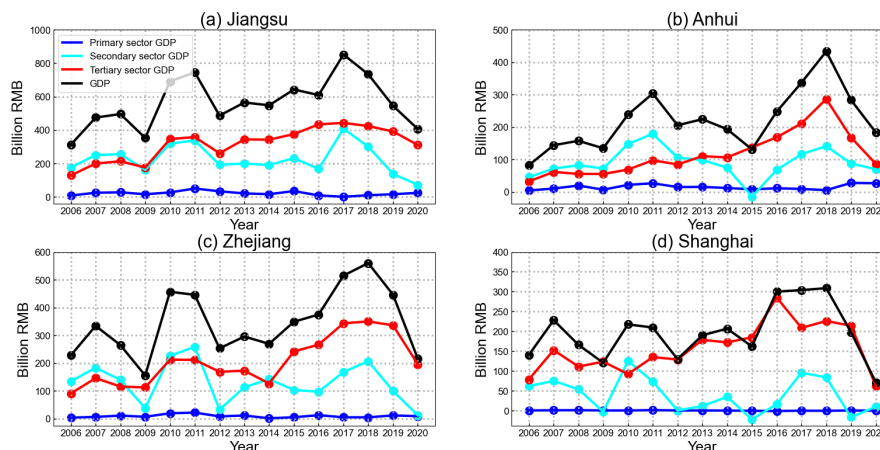


Figure 7. The same as Figure 6 but for annual average.



594



595

596 **Figure 8.** Time series of year-to-year increment in GDP, i.e., the increase in GDP at a given year
 597 relative to its previous year, over Jiangsu Province, Anhui Province, Zhejiang Province, and
 598 Shanghai within the YRD from 2006 to 2020. GDP for total, primary sector, secondary sector, and
 599 tertiary sector are marked with black, blue, cyan, and red dots/lines, respectively.

600



References

- Anand, J. S., and Monks, P. S.: Estimating daily surface NO₂ concentrations from satellite data – a case study over Hong Kong using land use regression models, *Atmos. Chem. Phys.*, 17, 8211–8230, 10.5194/acp-17-8211-2017, 2017.
- Baruah, U. D., Robeson, S. M., Saikia, A., Mili, N., Sung, K., and Chand, P.: Spatio-temporal characterization of tropospheric ozone and its precursor pollutants NO₂ and HCHO over South Asia, *Sci Total Environ*, 151135, <https://doi.org/10.1016/j.scitotenv.2021.151135>, 2021.
- Bechle, M. J., Millet, D. B., and Marshall, J. D.: Remote sensing of exposure to NO₂: Satellite versus ground-based measurement in a large urban area, *Atmos Environ*, 69, 345–353, <https://doi.org/10.1016/j.atmosenv.2012.11.046>, 2013.
- Boersma, K. F., Eskes, H. J., Veefkind, J. P., Brinksma, E. J., van der A, R. J., Sneep, M., van den Oord, G. H. J., Levelt, P. F., Stammes, P., Gleason, J. F., and Bucsela, E. J.: Near-real time retrieval of tropospheric NO₂ from OMI, *Atmos. Chem. Phys.*, 7, 2103–2118, 10.5194/acp-7-2103-2007, 2007.
- Boersma, K. F., Jacob, D. J., Trainic, M., Rudich, Y., DeSmedt, I., Dirksen, R., and Eskes, H. J.: Validation of urban NO₂ concentrations and their diurnal and seasonal variations observed from the SCIAMACHY and OMI sensors using in situ surface measurements in Israeli cities, *Atmos. Chem. Phys.*, 9, 3867–3879, 10.5194/acp-9-3867-2009, 2009.
- Boersma, K. F., Eskes, H. J., Dirksen, R. J., van der A, R. J., Veefkind, J. P., Stammes, P., Huijnen, V., Kleipool, Q. L., Sneep, M., Claas, J., Leitão, J., Richter, A., Zhou, Y., and Brunner, D.: An improved tropospheric NO₂ column retrieval algorithm for the Ozone Monitoring Instrument, *Atmos. Meas. Tech.*, 4, 1905–1928, 10.5194/amt-4-1905-2011, 2011.
- Bond, D. W., Zhang, R., Tie, X., Brasseur, G., Huffman, G., Orville, R. E., and Boccippio, D. J.: NO_x production by lightning over the continental United States, *Journal of Geophysical Research: Atmospheres*, 106, 27701–27710, <https://doi.org/10.1029/2000JD000191>, 2001.
- Browne, E. C., Min, K. E., Wooldridge, P. J., Apel, E., Blake, D. R., Brune, W. H., Cantrell, C. A., Cubison, M. J., Diskin, G. S., Jimenez, J. L., Weinheimer, A. J., Wennberg, P. O., Wisthaler, A., and Cohen, R. C.: Observations of total RONO₂ over the boreal forest: NO_x sinks and HNO₃ sources, *Atmos. Chem. Phys.*, 13, 4543–4562, 10.5194/acp-13-4543-2013, 2013.
- Bucsela, E. J., Krotkov, N. A., Celarier, E. A., Lamsal, L. N., Swartz, W. H., Bhartia, P. K., Boersma, K. F., Veefkind, J. P., Gleason, J. F., and Pickering, K. E.: A new stratospheric and tropospheric NO₂ retrieval algorithm for nadir-viewing satellite instruments: applications to OMI, *Atmos. Meas. Tech.*, 6, 2607–2626, 10.5194/amt-6-2607-2013, 2013.
- Carvalho, D.: An Assessment of NASA's GMAO MERRA-2 Reanalysis Surface Winds, *J Climate*, 32, 8261–8281, 10.1175/JCLI-D-19-0199.1, 2019.
- Cheng, M. M., Jiang, H., and Guo, Z.: Evaluation of long-term tropospheric NO₂ columns and the effect of different ecosystem in Yangtze River Delta, *Procedia Environmental Sciences*, 13, 1045–1056, <https://doi.org/10.1016/j.proenv.2012.01.098>, 2012.
- Chi, Y., Fan, M., Zhao, C., Sun, L., Yang, Y., Yang, X., and Tao, J.: Ground-level NO₂ concentration estimation based on OMI tropospheric NO₂ and its spatiotemporal characteristics in typical regions of China, *Atmos Res*, 264, 105821, <https://doi.org/10.1016/j.atmosres.2021.105821>, 2021.
- China State Council: the Air Pollution Prevention and Control Action Plan, http://www.gov.cn/zhengce/content/2013-09/13/content_4561.htm, 2013.
- Choi, Y., and Souri, A. H.: Chemical condition and surface ozone in large cities of Texas during the last decade: Observational evidence from OMI, CAMS, and model analysis, *Remote Sens Environ*, 168,



- 90-101, 2015.
- Cooper, M. J., Martin, R. V., McLinden, C. A., and Brook, J. R.: Inferring ground-level nitrogen dioxide concentrations at fine spatial resolution applied to the TROPOMI satellite instrument, *Environ Res Lett*, 15, 104013, [10.1088/1748-9326/aba3a5](https://doi.org/10.1088/1748-9326/aba3a5), 2020.
- Duncan, B. N., Yoshida, Y., de Foy, B., Lamsal, L. N., Streets, D. G., Lu, Z., Pickering, K. E., and Krotkov, N. A.: The observed response of Ozone Monitoring Instrument (OMI) NO₂ columns to NO_x emission controls on power plants in the United States: 2005–2011, *Atmos Environ*, 81, 102–111, <https://doi.org/10.1016/j.atmosenv.2013.08.068>, 2013.
- Duncan, B. N., Lamsal, L. N., Thompson, A. M., Yoshida, Y., Lu, Z., Streets, D. G., Hurwitz, M. M., and Pickering, K. E.: A space-based, high-resolution view of notable changes in urban NO_x pollution around the world (2005–2014), *Journal of Geophysical Research: Atmospheres*, 121, 976–996, <https://doi.org/10.1002/2015JD024121>, 2016.
- Geddes, J. A., Murphy, J. G., O'Brien, J. M., and Celarier, E. A.: Biases in long-term NO₂ averages inferred from satellite observations due to cloud selection criteria, *Remote Sens Environ*, 124, 210–216, <https://doi.org/10.1016/j.rse.2012.05.008>, 2012.
- Gelaro, R., McCarty, W., Suárez, M. J., Todling, R., Molod, A., Takacs, L., Randles, C. A., Darmenov, A., Bosilovich, M. G., Reichle, R., Wargan, K., Coy, L., Cullather, R., Draper, C., Akella, S., Buchard, V., Conaty, A., da Silva, A. M., Gu, W., Gi-Kong, K., Koster, R., Lucchesi, R., Merkova, D., Nielsen, J. E., Partyka, G., Pawson, S., Putman, W., Rienecker, M., Schubert, S. D., Sienkiewicz, M., and Zhao, B.: The Modern-Era Retrospective Analysis for Research and Applications, Version 2 (MERRA-2), *J Climate*, 30, 5419–5454, <http://dx.doi.org/10.1175/JCLI-D-16-0758.1>, 2017.
- Ghude, S. D., Van der A, R. J., Beig, G., Fadnavis, S., and Polade, S. D.: Satellite derived trends in NO₂ over the major global hotspot regions during the past decade and their inter-comparison, *Environmental Pollution*, 157, 1873–1878, <https://doi.org/10.1016/j.envpol.2009.01.013>, 2009.
- Ghude, S. D., Pfister, G. G., Jena, C., van der A, R. J., Emmons, L. K., and Kumar, R.: Satellite constraints of nitrogen oxide (NO_x) emissions from India based on OMI observations and WRF-Chem simulations, *Geophys Res Lett*, 40, 423–428, <https://doi.org/10.1002/grl.50065>, 2013.
- Goldberg, D. L., Lamsal, L. N., Loughner, C. P., Swartz, W. H., Lu, Z., and Streets, D. G.: A high-resolution and observationally constrained OMI NO₂ satellite retrieval, *Atmos. Chem. Phys.*, 17, 11403–11421, [10.5194/acp-17-11403-2017](https://doi.org/10.5194/acp-17-11403-2017), 2017.
- Guerriero, C., Chatzidiakou, L., Cairns, J., and Mumovic, D.: The economic benefits of reducing the levels of nitrogen dioxide (NO₂) near primary schools: The case of London, *Journal of Environmental Management*, 181, 615–622, <https://doi.org/10.1016/j.jenvman.2016.06.039>, 2016.
- Hakkarainen, J., Ialongo, I., and Tamminen, J.: Direct space-based observations of anthropogenic CO₂ emission areas from OCO-2, *Geophys Res Lett*, 43, 411,400–411,406, <https://doi.org/10.1002/2016GL070885>, 2016.
- Hakkarainen, J., Ialongo, I., Maksyutov, S., and Crisp, D.: Analysis of Four Years of Global XCO₂ Anomalies as Seen by Orbiting Carbon Observatory-2, *Remote Sens-Basel*, 11, 10.3390/rs11070850, 2019.
- He, J., Gong, S., Yu, Y., Yu, L., Wu, L., Mao, H., Song, C., Zhao, S., Liu, H., Li, X., and Li, R.: Air pollution characteristics and their relation to meteorological conditions during 2014–2015 in major Chinese cities, *Environmental Pollution*, 223, 484–496, <https://doi.org/10.1016/j.envpol.2017.01.050>, 2017.
- Hilboll, A., Richter, A., and Burrows, J. P.: Long-term changes of tropospheric NO₂ over megacities



- 689 derived from multiple satellite instruments, *Atmos. Chem. Phys.*, 13, 4145–4169, 10.5194/acp-13-
 690 4145-2013, 2013.
- 691 Jiang, Z., McDonald, B. C., Worden, H., Worden, J. R., Miyazaki, K., Qu, Z., Henze, D. K., Jones, D. B.
 692 A., Arellano, A. F., Fischer, E. V., Zhu, L. Y., and Boersma, K. F.: Unexpected slowdown of US
 693 pollutant emission reduction in the past decade, *P Natl Acad Sci USA*, 115, 5099–5104, 2018.
- 694 Jin, X., Fiore, A. M., Murray, L. T., Valin, L. C., Lamsal, L. N., Duncan, B., Folkert Boersma, K., De
 695 Smedt, I., Abad, G. G., Chance, K., and Tonnesen, G. S.: Evaluating a Space-Based Indicator of
 696 Surface Ozone-NO_x-VOC Sensitivity Over Midlatitude Source Regions and Application to Decadal
 697 Trends, *Journal of Geophysical Research: Atmospheres*, 122, 10,439–410,461,
 698 <https://doi.org/10.1002/2017JD026720>, 2017.
- 699 Jin, X., Fiore, A., Boersma, K. F., Smedt, I. D., and Valin, L.: Inferring Changes in Summertime Surface
 700 Ozone–NO_x–VOC Chemistry over U.S. Urban Areas from Two Decades of Satellite and Ground-
 701 Based Observations, *Environmental Science & Technology*, 54, 6518–6529,
 702 [10.1021/acs.est.9b07785](https://doi.org/10.1021/acs.est.9b07785), 2020.
- 703 Jin, X. M., and Holloway, T.: Spatial and temporal variability of ozone sensitivity over China observed
 704 from the Ozone Monitoring Instrument, *J Geophys Res-Atmos*, 120, 7229–7246, 2015.
- 705 Kharol, S. K., Martin, R. V., Philip, S., Boys, B., Lamsal, L. N., Jerrett, M., Brauer, M., Crouse, D. L.,
 706 McLinden, C., and Burnett, R. T.: Assessment of the magnitude and recent trends in satellite-derived
 707 ground-level nitrogen dioxide over North America, *Atmos Environ*, 118, 236–245,
 708 <https://doi.org/10.1016/j.atmosenv.2015.08.011>, 2015.
- 709 Kim, D.-R., Lee, J.-B., Keun Song, C., Kim, S.-Y., Ma, Y.-I., Lee, K.-M., Cha, J.-S., and Lee, S.-D.:
 710 Temporal and spatial distribution of tropospheric NO₂ over Northeast Asia using OMI data during
 711 the years 2005–2010, *Atmospheric Pollution Research*, 6, 768–776,
 712 <https://doi.org/10.5094/APR.2015.085>, 2015.
- 713 Kishore Kumar, G., Kishore Kumar, K., Baumgarten, G., and Ramkumar, G.: Validation of MERRA
 714 reanalysis upper-level winds over low latitudes with independent rocket sounding data, *J Atmos*
 715 *Sol-Terr Phy*, 123, 48–54, <https://doi.org/10.1016/j.jastp.2014.12.001>, 2015.
- 716 Kramer, L. J., Leigh, R. J., Remedios, J. J., and Monks, P. S.: Comparison of OMI and ground-based in
 717 situ and MAX-DOAS measurements of tropospheric nitrogen dioxide in an urban area, *Journal of*
 718 *Geophysical Research: Atmospheres*, 113, <https://doi.org/10.1029/2007JD009168>, 2008.
- 719 Krotkov, N. A., McLinden, C. A., Li, C., Lamsal, L. N., Celarier, E. A., Marchenko, S. V., Swartz, W. H.,
 720 Bucsela, E. J., Joiner, J., Duncan, B. N., Boersma, K. F., Veefkind, J. P., Levelt, P. F., Fioletov, V.
 721 E., Dickerson, R. R., He, H., Lu, Z., and Streets, D. G.: Aura OMI observations of regional SO₂ and
 722 NO₂ pollution changes from 2005 to 2015, *Atmos. Chem. Phys.*, 16, 4605–4629, 10.5194/acp-16-
 723 4605-2016, 2016.
- 724 Lamsal, L. N., Martin, R. V., van Donkelaar, A., Steinbacher, M., Celarier, E. A., Bucsela, E., Dunlea, E.
 725 J., and Pinto, J. P.: Ground-level nitrogen dioxide concentrations inferred from the satellite-borne
 726 Ozone Monitoring Instrument, *Journal of Geophysical Research: Atmospheres*, 113,
 727 <https://doi.org/10.1029/2007JD009235>, 2008.
- 728 Lamsal, L. N., Krotkov, N. A., Celarier, E. A., Swartz, W. H., Pickering, K. E., Bucsela, E. J., Gleason,
 729 J. F., Martin, R. V., Philip, S., Irie, H., Cede, A., Herman, J., Weinheimer, A., Szykman, J. J., and
 730 Knepp, T. N.: Evaluation of OMI operational standard NO₂ column retrievals using in situ and
 731 surface-based NO₂ observations, *Atmos. Chem. Phys.*, 14, 11587–11609, 10.5194/acp-14-11587-
 732 2014, 2014.



- Lamsal, L. N., Duncan, B. N., Yoshida, Y., Krotkov, N. A., Pickering, K. E., Streets, D. G., and Lu, Z.: U.S. NO₂ trends (2005–2013): EPA Air Quality System (AQS) data versus improved observations from the Ozone Monitoring Instrument (OMI), *Atmos Environ*, 110, 130–143, <https://doi.org/10.1016/j.atmosenv.2015.03.055>, 2015.
- Levelt, P. F., Oord, G. H. J. v. d., Dobber, M. R., Malkki, A., Huib, V., Johan de, V., Stammes, P., Lundell, J. O. V., and Saari, H.: The ozone monitoring instrument, *IEEE Transactions on Geoscience and Remote Sensing*, 44, 1093–1101, 10.1109/TGRS.2006.872333, 2006.
- Li, K., Jacob, D. J., Liao, H., Shen, L., Zhang, Q., and Bates, K. H.: Anthropogenic drivers of 2013–2017 trends in summer surface ozone in China, *Proceedings of the National Academy of Sciences*, 116, 422, 10.1073/pnas.1812168116, 2019.
- Li, K., Jacob, D. J., Shen, L., Lu, X., De Smedt, I., and Liao, H.: Increases in surface ozone pollution in China from 2013 to 2019: anthropogenic and meteorological influences, *Atmos. Chem. Phys.*, 20, 11423–11433, 10.5194/acp-20-11423-2020, 2020.
- Li, R., Xu, M., Li, M., Chen, Z., Zhao, N., Gao, B., and Yao, Q.: Identifying the spatiotemporal variations in ozone formation regimes across China from 2005 to 2019 based on polynomial simulation and causality analysis, *Atmos. Chem. Phys.*, 21, 15631–15646, 10.5194/acp-21-15631-2021, 2021.
- Lin, C., Lau, A. K. H., Fung, J. C. H., Song, Y., Li, Y., Tao, M., Lu, X., Ma, J., and Lao, X. Q.: Removing the effects of meteorological factors on changes in nitrogen dioxide and ozone concentrations in China from 2013 to 2020, *Sci Total Environ*, 793, 148575, <https://doi.org/10.1016/j.scitotenv.2021.148575>, 2021.
- Lin, J., Nielsen, C. P., Zhao, Y., Lei, Y., Liu, Y., and McElroy, M. B.: Recent Changes in Particulate Air Pollution over China Observed from Space and the Ground: Effectiveness of Emission Control, *Environmental Science & Technology*, 44, 7771–7776, 10.1021/es101094t, 2010.
- Lin, J. T., and McElroy, M. B.: Detection from space of a reduction in anthropogenic emissions of nitrogen oxides during the Chinese economic downturn, *Atmos. Chem. Phys.*, 11, 8171–8188, 10.5194/acp-11-8171-2011, 2011.
- Liu, F., Zhang, Q., van der A, R. J., Zheng, B., Tong, D., Yan, L., Zheng, Y., and He, K.: Recent reduction in NO_x emissions over China: synthesis of satellite observations and emission inventories, *Environ Res Lett*, 11, 114002, 10.1088/1748-9326/11/11/114002, 2016.
- Liu, F., Beirle, S., Zhang, Q., van der A, R. J., Zheng, B., Tong, D., and He, K.: NO_x emission trends over Chinese cities estimated from OMI observations during 2005 to 2015, *Atmos. Chem. Phys.*, 17, 9261–9275, 10.5194/acp-17-9261-2017, 2017.
- Liu, F., van der A, R. J., Eskes, H., Ding, J., and Mijling, B.: Evaluation of modeling NO₂ concentrations driven by satellite-derived and bottom-up emission inventories using in situ measurements over China, *Atmos. Chem. Phys.*, 18, 4171–4186, 10.5194/acp-18-4171-2018, 2018.
- Lu, X., Zhang, L., Chen, Y., Zhou, M., Zheng, B., Li, K., Liu, Y., Lin, J., Fu, T. M., and Zhang, Q.: Exploring 2016–2017 surface ozone pollution over China: source contributions and meteorological influences, *Atmos. Chem. Phys.*, 19, 8339–8361, 10.5194/acp-19-8339-2019, 2019a.
- Lu, X., Zhang, L., and Shen, L.: Meteorology and Climate Influences on Tropospheric Ozone: a Review of Natural Sources, Chemistry, and Transport Patterns, *Current Pollution Reports*, 5, 238–260, 10.1007/s40726-019-00118-3, 2019b.
- Lu, X., Zhang, L., Wang, X., Gao, M., Li, K., Zhang, Y., Yue, X., and Zhang, Y.: Rapid Increases in Warm-Season Surface Ozone and Resulting Health Impact in China Since 2013, *Environ Sci Tech Lett*, 7, 240–247, 10.1021/acs.estlett.0c00171, 2020.



- 777 Lu, X., Ye, X., Zhou, M., Zhao, Y., Weng, H., Kong, H., Li, K., Gao, M., Zheng, B., Lin, J., Zhou, F.,
 778 Zhang, Q., Wu, D., Zhang, L., and Zhang, Y.: The underappreciated role of agricultural soil nitrogen
 779 oxide emissions in ozone pollution regulation in North China, *Nature Communications*, 12, 5021,
 780 10.1038/s41467-021-25147-9, 2021.
- 781 Lu, Z., Streets, D. G., de Foy, B., Lamsal, L. N., Duncan, B. N., and Xing, J.: Emissions of nitrogen
 782 oxides from US urban areas: estimation from Ozone Monitoring Instrument retrievals for 2005–
 783 2014, *Atmos. Chem. Phys.*, 15, 10367–10383, 10.5194/acp-15-10367-2015, 2015.
- 784 MacIntyre, E. A., Gehring, U., Mölter, A., Fuertes, E., Klümper, C., Krämer, U., Quass, U., Hoffmann,
 785 B., Gascon, M., Brunekreef, B., Koppelman, G. H., Beelen, R., Hoek, G., Birk, M., de Jongste, J.
 786 C., Smit, H. A., Cyrus, J., Gruzicova, O., Korek, M., Bergström, A., Agius, R. M., de Vocht, F.,
 787 Simpson, A., Porta, D., Forastiere, F., Badaloni, C., Cesaroni, G., Esplugues, A., Fernández-
 788 Somoano, A., Lerxundi, A., Sunyer, J., Cirach, M., Nieuwenhuijsen, M. J., Pershagen, G., and
 789 Heinrich, J.: Air pollution and respiratory infections during early childhood: An analysis of 10
 790 European birth cohorts within the ESCAPE project, *Environmental Health Perspectives*, 122, 107–
 791 113, 10.1289/ehp.1306755, 2014.
- 792 Marchenko, S., Krotkov, N. A., Lamsal, L. N., Celarier, E. A., Swartz, W. H., and Bucsela, E. J.: Revising
 793 the slant column density retrieval of nitrogen dioxide observed by the Ozone Monitoring Instrument,
 794 *Journal of Geophysical Research: Atmospheres*, 120, 5670–5692,
 795 <https://doi.org/10.1002/2014JD022913>, 2015.
- 796 Meng, X., Liu, C., Chen, R. J., Sera, F., Vicedo-Cabrera, A. M., Milojevic, A., Guo, Y. M., Tong, S. L.,
 797 Coelho, M. D. Z. S., Saldiva, P. H. N., Lavigne, E., Correa, P. M., Ortega, N. V., Garcia, S. O.,
 798 Kysely, J., Urban, A., Orru, H., Maasikmets, M., Jaakkola, J. J. K., Rytty, N., Huber, V., Schneider,
 799 A., Katsouyanni, K., Analitis, A., Hashizume, M., Honda, Y., Ng, C. F. S., Nunes, B., Teixeira, J. P.,
 800 Holobaca, I. H., Fratianni, S., Kim, H., Tobias, A., Iniguez, C., Forsberg, B., Astrom, C., Ragetti,
 801 M. S., Guo, Y. L. L., Pan, S. C., Li, S. S., Bell, M. L., Zanobetti, A., Schwartz, J., Wu, T. C.,
 802 Gasparri, A., and Kan, H. D.: Short term associations of ambient nitrogen dioxide with daily total,
 803 cardiovascular, and respiratory mortality: multilocation analysis in 398 cities, *Bmj-Brit Med J*, 372,
 804 2021.
- 805 Meng, Z.-Y., Xu, X.-B., Wang, T., Zhang, X.-Y., Yu, X.-L., Wang, S.-F., Lin, W.-L., Chen, Y.-Z., Jiang,
 806 Y.-A., and An, X.-Q.: Ambient sulfur dioxide, nitrogen dioxide, and ammonia at ten background
 807 and rural sites in China during 2007–2008, *Atmos Environ*, 44, 2625–2631,
 808 <https://doi.org/10.1016/j.atmosenv.2010.04.008>, 2010.
- 809 Ministry of Ecology and Environment of the People's Republic of China: Limits and measurement
 810 methods for emissions from light-duty vehicles (III , IV),
 811 http://www.mee.gov.cn/ywggz/fgbz/bzwb/dqjhjbh/dqdywrrwfbz/200707/t20070701_66145.shtm, 2007.
- 813 Ministry of Ecology and Environment of the People's Republic of China: Announcement on the
 814 implementation of the national phase IV vehicle compression ignition engine and vehicle pollutant
 815 emission standards, https://www.mee.gov.cn/gkml/hbb/bgg/201201/t20120110_222376.htm, 2011.
- 816 Ministry of Ecology and Environment of the People's Republic of China: Announcement on the
 817 implementation of phase V motor vehicle emission standards,,
 818 https://www.mee.gov.cn/gkml/hbb/bgg/201601/t20160118_326596.htm, 2016.
- 819 Ministry of Ecology and Environment of the People's Republic of China: Limits and measurement
 820 methods for emissions from light-duty vehicles (CHINA 5),



- 821 http://www.mee.gov.cn/ywgz/fgbz/bz/bzwb/dqhjbh/dqdywrwpfbz/201309/t20130917_260352.sh
 822 tml, 2018.
- 823 Mustafa, F., Bu, L., Wang, Q., Yao, N., Shahzaman, M., Bilal, M., Aslam, R. W., and Iqbal, R.: Neural-
 824 network-based estimation of regional-scale anthropogenic CO₂ emissions using an Orbiting Carbon
 825 Observatory-2 (OCO-2) dataset over East and West Asia, *Atmos. Meas. Tech.*, 14, 7277-7290,
 826 10.5194/amt-14-7277-2021, 2021.
- 827 Pearce, J. L., Beringer, J., Nicholls, N., Hyndman, R. J., and Tapper, N. J.: Quantifying the influence of
 828 local meteorology on air quality using generalized additive models, *Atmos Environ*, 45, 1328-1336,
 829 <https://doi.org/10.1016/j.atmosenv.2010.11.051>, 2011.
- 830 Richter, A., Burrows, J. P., Nüß, H., Granier, C., and Niemeier, U.: Increase in tropospheric nitrogen
 831 dioxide over China observed from space, *Nature*, 437, 129-132, 10.1038/nature04092, 2005.
- 832 Rotman, D. A., Tannahill, J. R., Kinnison, D. E., Connell, P. S., Bergmann, D., Proctor, D., Rodriguez, J.
 833 M., Lin, S. J., Rood, R. B., Prather, M. J., Rasch, P. J., Considine, D. B., Ramaroson, R., and Kawa,
 834 S. R.: Global Modeling Initiative assessment model: Model description, integration, and testing of
 835 the transport shell, *Journal of Geophysical Research: Atmospheres*, 106, 1669-1691,
 836 <https://doi.org/10.1029/2000JD900463>, 2001.
- 837 Russell, A. R., Valin, L. C., and Cohen, R. C.: Trends in OMI NO₂ observations over the United States:
 838 effects of emission control technology and the economic recession, *Atmos. Chem. Phys.*, 12, 12197-
 839 12209, 10.5194/acp-12-12197-2012, 2012.
- 840 Schreier, S. F., Peters, E., Richter, A., Lampel, J., Wittrock, F., and Burrows, J. P.: Ship-based MAX-
 841 DOAS measurements of tropospheric NO₂ and SO₂ in the South China and Sulu Sea, *Atmos Environ*,
 842 102, 331-343, <https://doi.org/10.1016/j.atmosenv.2014.12.015>, 2015.
- 843 Schroeder, J. R., Crawford, J. H., Fried, A., Walega, J., Weinheimer, A., Wisthaler, A., Muller, M.,
 844 Mikoviny, T., Chen, G., Shook, M., Blake, D. R., and Tonnesen, G. S.: New insights into the column
 845 CH₂O/NO₂ ratio as an indicator of near-surface ozone sensitivity, *J Geophys Res-Atmos*, 122, 8885-
 846 8907, 2017.
- 847 Shaiganfar, R., Beirle, S., Denier van der Gon, H., Jonkers, S., Kuenen, J., Petetin, H., Zhang, Q.,
 848 Beekmann, M., and Wagner, T.: Estimation of the Paris NO_x emissions from mobile MAX-DOAS
 849 observations and CHIMERE model simulations during the MEGAPOLI campaign using the closed
 850 integral method, *Atmos. Chem. Phys.*, 17, 7853-7890, 10.5194/acp-17-7853-2017, 2017.
- 851 Silvern, R. F., Jacob, D. J., Mickley, L. J., Sulprizio, M. P., Travis, K. R., Marais, E. A., Cohen, R. C.,
 852 Laughner, J. L., Choi, S., Joiner, J., and Lamsal, L. N.: Using satellite observations of tropospheric
 853 NO₂ columns to infer long-term trends in US NO_x emissions: the importance of accounting for the
 854 free tropospheric NO₂ background, *Atmos. Chem. Phys.*, 19, 8863-8878, 10.5194/acp-19-8863-
 855 2019, 2019.
- 856 Solomon, S., Schmeltekopf, A. L., and Sanders, R. W.: On the interpretation of zenith sky absorption
 857 measurements, *Journal of Geophysical Research: Atmospheres*, 92, 8311-8319,
 858 <https://doi.org/10.1029/JD092iD07p08311>, 1987.
- 859 Song, Z., Fu, D., Zhang, X., Wu, Y., Xia, X., He, J., Han, X., Zhang, R., and Che, H.: Diurnal and seasonal
 860 variability of PM_{2.5} and AOD in North China plain: Comparison of MERRA-2 products and ground
 861 measurements, *Atmos Environ*, 191, 70-78, <https://doi.org/10.1016/j.atmosenv.2018.08.012>, 2018.
- 862 Sourì, A. H., Choi, Y., Jeon, W., Woo, J.-H., Zhang, Q., and Kurokawa, J.-i.: Remote sensing evidence
 863 of decadal changes in major tropospheric ozone precursors over East Asia, *Journal of Geophysical*
 864 *Research: Atmospheres*, 122, 2474-2492, <https://doi.org/10.1002/2016JD025663>, 2017.



- Streets, D. G., Canty, T., Carmichael, G. R., de Foy, B., Dickerson, R. R., Duncan, B. N., Edwards, D. P., Haynes, J. A., Henze, D. K., Houyoux, M. R., Jacob, D. J., Krotkov, N. A., Lamsal, L. N., Liu, Y., Lu, Z., Martin, R. V., Pfister, G. G., Pinder, R. W., Salawitch, R. J., and Wecht, K. J.: Emissions estimation from satellite retrievals: A review of current capability, *Atmos Environ*, 77, 1011-1042, <https://doi.org/10.1016/j.atmosenv.2013.05.051>, 2013.
- Sun, Y., Liu, C., Zhang, L., Palm, M., Notholt, J., Yin, H., Vigouroux, C., Lutsch, E., Wang, W., Shan, C., Blumenstock, T., Nagahama, T., Morino, I., Mahieu, E., Strong, K., Langerock, B., De Mazière, M., Hu, Q., Zhang, H., Petri, C., and Liu, J.: Fourier transform infrared time series of tropospheric HCN in eastern China: seasonality, interannual variability, and source attribution, *Atmos. Chem. Phys.*, 20, 5437-5456, 10.5194/acp-20-5437-2020, 2020.
- Sun, Y., Yin, H., Liu, C., Zhang, L., Cheng, Y., Palm, M., Notholt, J., Lu, X., Vigouroux, C., Zheng, B., Wang, W., Jones, N., Shan, C., Qin, M., Tian, Y., Hu, Q., Meng, F., and Liu, J.: Mapping the drivers of formaldehyde (HCHO) variability from 2015 to 2019 over eastern China: insights from Fourier transform infrared observation and GEOS-Chem model simulation, *Atmos. Chem. Phys.*, 21, 6365-6387, 10.5194/acp-21-6365-2021, 2021a.
- Sun, Y., Yin, H., Lu, X., Notholt, J., Palm, M., Liu, C., Tian, Y., and Zheng, B.: The drivers and health risks of the unexpected surface ozone enhancements over the Sichuan basin, China in 2020, *Atmos. Chem. Phys. Discuss.*, 2021, 1-29, 10.5194/acp-2021-664, 2021b.
- Sun, Y., Yin, H., Cheng, Y., Zhang, Q., Zheng, B., Notholt, J., Lu, X., Liu, C., Tian, Y., and Liu, J.: Quantifying variability, source, and transport of CO in the urban areas over the Himalayas and Tibetan Plateau, *Atmos. Chem. Phys.*, 21, 9201-9222, 10.5194/acp-21-9201-2021, 2021c.
- Sun, Y. W., Liu, C., Palm, M., Vigouroux, C., Notholt, J., Hui, Q. H., Jones, N., Wang, W., Su, W. J., Zhang, W. Q., Shan, C. G., Tian, Y., Xu, X. W., De Mazière, M., Zhou, M. Q., and Liu, J. G.: Ozone seasonal evolution and photochemical production regime in the polluted troposphere in eastern China derived from high-resolution Fourier transform spectrometry (FTS) observations, *Atmos Chem Phys*, 18, 14569-14583, 2018.
- Tao, Y., Huang, W., Huang, X., Zhong, L., Lu, S. E., Li, Y., Dai, L., Zhang, Y., and Zhu, T.: Estimated acute effects of ambient ozone and nitrogen dioxide on mortality in the Pearl River Delta of southern China, *Environmental Health Perspectives*, 120, 393-398, 10.1289/ehp.1103715, 2012.
- van Geffen, J. H. G. M., Boersma, K. F., Van Roozendaal, M., Hendrick, F., Mahieu, E., De Smedt, I., Sneep, M., and Veefkind, J. P.: Improved spectral fitting of nitrogen dioxide from OMI in the 405–465 nm window, *Atmos. Meas. Tech.*, 8, 1685-1699, 10.5194/amt-8-1685-2015, 2015.
- Vrekoussis, M., Richter, A., Hilboll, A., Burrows, J. P., Gerasopoulos, E., Lelieveld, J., Barrie, L., Zerefos, C., and Mihalopoulos, N.: Economic crisis detected from space: Air quality observations over Athens/Greece, *Geophys Res Lett*, 40, 458-463, <https://doi.org/10.1002/grl.50118>, 2013.
- Wallace, J., and Kanaroglou, P.: The sensitivity of OMI-derived nitrogen dioxide to boundary layer temperature inversions, *Atmos Environ*, 43, 3596-3604, <https://doi.org/10.1016/j.atmosenv.2009.03.049>, 2009.
- Wang, S., Xing, J., Chatani, S., Hao, J., Klimont, Z., Cofala, J., and Amann, M.: Verification of anthropogenic emissions of China by satellite and ground observations, *Atmos Environ*, 45, 6347-6358, <https://doi.org/10.1016/j.atmosenv.2011.08.054>, 2011.
- Wang, Y., Yang, K., Pan, Z., Qin, J., Chen, D., Lin, C., Chen, Y., Lazhu, Tang, W., Han, M., Lu, N., and Wu, H.: Evaluation of Precipitable Water Vapor from Four Satellite Products and Four Reanalysis Datasets against GPS Measurements on the Southern Tibetan Plateau, *J Climate*, 30, 5699-5713,



- 10.1175/JCLI-D-16-0630.1, 2017.
- Xu, W. Y., Zhao, C. S., Ran, L., Deng, Z. Z., Liu, P. F., Ma, N., Lin, W. L., Xu, X. B., Yan, P., He, X., Yu, J., Liang, W. D., and Chen, L. L.: Characteristics of pollutants and their correlation to meteorological conditions at a suburban site in the North China Plain, *Atmos. Chem. Phys.*, 11, 4353-4369, 10.5194/acp-11-4353-2011, 2011.
- Xue, R., Wang, S., Li, D., Zou, Z., Chan, K. L., Valks, P., Saiz-Lopez, A., and Zhou, B.: Spatio-temporal variations in NO₂ and SO₂ over Shanghai and Chongming Eco-Island measured by Ozone Monitoring Instrument (OMI) during 2008–2017, *Journal of Cleaner Production*, 258, 120563, <https://doi.org/10.1016/j.jclepro.2020.120563>, 2020.
- Yin, H., Sun, Y., Liu, C., Zhang, L., Lu, X., Wang, W., Shan, C., Hu, Q., Tian, Y., Zhang, C., Su, W., Zhang, H., Palm, M., Notholt, J., and Liu, J.: FTIR time series of stratospheric NO₂ over Hefei, China, and comparisons with OMI and GEOS-Chem model data, *Opt Express*, 27, A1225-A1240, 10.1364/OE.27.0A1225, 2019.
- Yin, H., Sun, Y., Liu, C., Lu, X., Smale, D., Blumenstock, T., Nagahama, T., Wang, W., Tian, Y., Hu, Q., Shan, C., Zhang, H., and Liu, J.: Ground-based FTIR observation of hydrogen chloride (HCl) over Hefei, China, and comparisons with GEOS-Chem model data and other ground-based FTIR stations data, *Opt Express*, 28, 8041-8055, 10.1364/OE.384377, 2020.
- Yin, H., Liu, C., Hu, Q., Liu, T., Wang, S., Gao, M., Xu, S., Zhang, C., and Su, W.: Opposite impact of emission reduction during the COVID-19 lockdown period on the surface concentrations of PM_{2.5} and O₃ in Wuhan, China, *Environmental Pollution*, 289, 117899, <https://doi.org/10.1016/j.envpol.2021.117899>, 2021a.
- Yin, H., Lu, X., Sun, Y., Li, K., Gao, M., Zheng, B., and Liu, C.: Unprecedented decline in summertime surface ozone over eastern China in 2020 comparably attributable to anthropogenic emission reductions and meteorology, *Environ Res Lett*, 2021b.
- Yin, H., Sun, Y., Liu, C., Wang, W., Shan, C., and Zha, L.: Remote Sensing of Atmospheric Hydrogen Fluoride (HF) over Hefei, China with Ground-Based High-Resolution Fourier Transform Infrared (FTIR) Spectrometry, *Remote Sens-Basel*, 13, 791, 2021c.
- Yin, H., Sun, Y., Wang, W., Shan, C., Tian, Y., and Liu, C.: Ground-based high-resolution remote sensing of sulphur hexafluoride (SF₆) over Hefei, China: characterization, optical misalignment, influence, and variability, *Opt Express*, 29, 34051-34065, 10.1364/OE.440193, 2021d.
- Zhai, S., Jacob, D. J., Wang, X., Shen, L., Li, K., Zhang, Y., Gui, K., Zhao, T., and Liao, H.: Fine particulate matter (PM_{2.5}) trends in China, 2013–2018: separating contributions from anthropogenic emissions and meteorology, *Atmos. Chem. Phys.*, 19, 11031-11041, 10.5194/acp-19-11031-2019, 2019.
- Zhang, L., Lee, C. S., Zhang, R., and Chen, L.: Spatial and temporal evaluation of long term trend (2005–2014) of OMI retrieved NO₂ and SO₂ concentrations in Henan Province, China, *Atmos Environ*, 154, 151-166, <https://doi.org/10.1016/j.atmosenv.2016.11.067>, 2017.
- Zhang, R., Tie, X., and Bond, D. W.: Impacts of anthropogenic and natural NO_x sources over the U.S. on tropospheric chemistry, *Proceedings of the National Academy of Sciences*, 100, 1505, 10.1073/pnas.252763799, 2003.
- Zhang, S., Wang, S., Zhang, R., Guo, Y., Yan, Y., Ding, Z., and Zhou, B.: Investigating the Sources of Formaldehyde and Corresponding Photochemical Indications at a Suburb Site in Shanghai From MAX-DOAS Measurements, *Journal of Geophysical Research: Atmospheres*, 126, e2020JD033351, <https://doi.org/10.1029/2020JD033351>, 2021.



- 953 Zhao, S., Yu, Y., Yin, D., He, J., Liu, N., Qu, J., and Xiao, J.: Annual and diurnal variations of gaseous
 954 and particulate pollutants in 31 provincial capital cities based on in situ air quality monitoring data
 955 from China National Environmental Monitoring Center, *Environment International*, 86, 92-106,
 956 <https://doi.org/10.1016/j.envint.2015.11.003>, 2016.
- 957 Zhao, Z., and Wang, Y.: Influence of the West Pacific subtropical high on surface ozone daily variability
 958 in summertime over eastern China, *Atmos Environ*, 170, 197-204,
 959 <https://doi.org/10.1016/j.atmosenv.2017.09.024>, 2017.
- 960 Zheng, B., Tong, D., Li, M., Liu, F., Hong, C., Geng, G., Li, H., Li, X., Peng, L., Qi, J., Yan, L., Zhang,
 961 Y., Zhao, H., Zheng, Y., He, K., and Zhang, Q.: Trends in China's anthropogenic emissions since
 962 2010 as the consequence of clean air actions, *Atmos. Chem. Phys.*, 18, 14095-14111, 10.5194/acp-
 963 18-14095-2018, 2018a.
- 964 Zheng, C., Zhao, C., Li, Y., Wu, X., Zhang, K., Gao, J., Qiao, Q., Ren, Y., Zhang, X., and Chai, F.: Spatial
 965 and temporal distribution of NO₂ and SO₂ in Inner Mongolia urban agglomeration obtained from
 966 satellite remote sensing and ground observations, *Atmos Environ*, 188, 50-59,
 967 <https://doi.org/10.1016/j.atmosenv.2018.06.029>, 2018b.
- 968 Zheng, F., Yu, T., Cheng, T., Gu, X., and Guo, H.: Intercomparison of tropospheric nitrogen dioxide
 969 retrieved from Ozone Monitoring Instrument over China, *Atmospheric Pollution Research*, 5, 686-
 970 695, <https://doi.org/10.5094/APR.2014.078>, 2014.
- 971 Zhou, C., Wang, K., and Ma, Q.: Evaluation of Eight Current Reanalyses in Simulating Land Surface
 972 Temperature from 1979 to 2003 in China, *J Climate*, 30, 7379-7398, 10.1175/JCLI-D-16-0903.1,
 973 2017.
 974